A STUDY OF THE NUCLEUS USING RELATIVISTIC WAVE FUNCTIONS

By

JEFFREY JOHN BRAUN

Bachelor of Arts

Knox College

Galesburg, Illinois

1967

Submitted to the Faculty of the Graduate College
of the Oklahoma State University
in partial fulfillment of the requirements
for the Degree of
MASTER OF SCIENCE
May, 1970

A STUDY OF THE NUCLEUS USING

RELATIVISTIC WAVE FUNCTIONS

Thesis Approved:

N. V. V. J. Swamy

Thesis Adviser

Arlo R. Schmidt

Mark Samuel

D. Durham

Dean of the Graduate College

PREFACE

In this study, an equivalent harmonic oscillator using relativistic wave functions was used as a single-particle nuclear model. The energy levels, radial densities, and elastic scattering cross-sections have been calculated and compared with the non-relativistic harmonic oscillator model and with experiment. The results obtained did not correlate well with experimental data, and this has been interpreted as further proof that the nucleons do not move with relativistic motions.

I would like to thank Dr. N. V. V. J. Swamy for his suggestion of the problem and his patient guidance during the course of this work. I would also like to acknowledge the financial support of the OSU Research Foundation.

TABLE OF CONTENTS

Chapter		Page
I.	INTRODUCTION.	1
II.	THE EHO HAMILTONIAN AND SOLUTIONS	4
	The Non-Relativistic Harmonic Oscillator	4
	The Spin-Angle Function.	6
	Non-Relativistic Limit of H_{EHO}	11
	Free-Particle Limit of H_{EHO}.	12
	Relation of the EHO to the Nilsson Hamiltonian . . .	15
III.	THE EHO AS A NUCLEAR MODEL.	18
IV.	COMPARISON OF THE EHO WITH EXPERIMENT	24
	Radial Density of the EHO.	24
	Determination of the Oscillator Parameter.	29
	Review of Experimental Work in Elastic Scattering of Electrons.	31
	Radial Densities	35
	Theory of Electron Scattering.	43
V.	CONCLUSIONS	67
REFERENCES.	. . . . .	71
APPENDIX A.	NORMALIZED RADIAL EIGENFUNCTIONS OF THE NRHO	74
APPENDIX B.	THE SPIN-ANGLE FUNCTIONS	76
APPENDIX C.	PROGRAM FOR COEFFICIENTS IN $\rho(r)$, $d\sigma/d\Omega$.	78
APPENDIX D.	PROGRAM FOR STURM SERIES	83
APPENDIX E.	PROGRAM FOR EVALUATION OF $d\sigma/d\Omega$.	88

LIST OF TABLES

Table		Page
I.	Degeneracy of the EHO and the NRHO.	19
II.	Ordering of States in the EHO	22
III.	Coefficients in the Densities of Selected Nuclei.	27
IV.	Oscillator Parameters for the Nuclei Under Study.	35
V.	Phenomenological Densities.	37
VI.	Coefficients in the Form Factor of Selected Nuclei. . . .	49
VII.	Zeros of the Form Factor.	51

LIST OF FIGURES

Figure		Page
1.	Proton Density in He^4	38
2.	Proton Density in C^{12}	39
3.	Proton Density in Ca^{40}	40
4.	Proton Density in In^{115}	41
5.	Proton Density in Pb^{208}	42
6.	Absolute Value of the Form Factor for He^4	52
7.	Absolute Value of the Form Factor for C^{12}	53
8.	Absolute Value of the Form Factor for Ca^{40}	54
9.	Absolute Value of the Form Factor for In^{115}	55
10.	Absolute Value of the Form Factor for Pb^{208}	56
11.	Differential Cross-Sections for Elastic Scattering of 800 MeV Electrons by Helium	59
12.	Differential Cross-Sections for Elastic Scattering of 600 MeV Electrons by Carbon	60
13.	Differential Cross-Sections for Elastic Scattering of 183 MeV Electrons by Calcium	61
14.	Differential Cross-Sections for Elastic Scattering of 250 MeV Electrons by Calcium	62
15.	Differential Cross-Sections for Elastic Scattering of 757.5 MeV Electrons by Calcium	63
16.	Differential Cross-Sections for Elastic Scattering of 183 MeV Electrons by Indium	64
17.	Differential Cross-Sections for Elastic Scattering of 248 MeV Electrons by Lead	65
18.	Differential Cross-Sections for Elastic Scattering of 502 MeV Electrons by Lead	66

CHAPTER I

INTRODUCTION

While there is certainly no dearth of nuclear models, we feel that the relativistic equivalent harmonic oscillator (EHO) is a valuable and interesting addition. The lack of any relativistic single-particle model till now prompted us to investigate some of the properties of the EHO.

Nearly all of the relativistic models of the nucleus before the EHO were studied about 20 or 30 years ago. Use of relativity in explaining nuclear phenomena fell into disfavor after this initial interest subsided, and we have found that all the work done in this area was performed between 1935 and 1950.

One of the earliest uses of relativity was made by Blochinzew (1) and later amplified by Margenau (2). In these papers, the Klein-Gordon equation was applied to a study of the deuteron binding energy. Using two different potentials (a rectangular potential hole and an error function potential) the zero-point energy of the neutron-proton system was calculated. If the range of the force is assumed to be 1 fermi, the zero-point energy is then five times the binding energy, while if the range of the force is assumed to 3 fermis, the zero-point energy is then only 13% of the binding energy. In 1936, Feenberg (3) again studied the deuteron, looking at relativistic corrections to the kinetic energy operator in the Schroedinger equation. For deuteron, the correction

led to a change of 25% of the energy predicted by the non-relativistic single-particle theory. Studying also triton and helium, he found the corrections to be $\Delta E \sim - .2\ mc^2$ and $\Delta E \sim - .9\ mc^2$, respectively. Applying a more rigorous treatment involving Dirac operators, Share and Breit (4) utilized two Dirac Hamiltonians for the two particles in the deuteron and an interaction represented by Dirac operators as well. Utilizing the relativistic formalism of the Dirac operators, they considered terms in the deuteron Hamiltonian which represented interactions between the orbits of the two particles, and the relativistic corrections to the particles' kinetic energies (such as those considered in references (1) - (3)) are seen to be small as compared to the changes required by a completely relativistic Dirac Hamiltonian. Primakoff (5) considered the Pauli magnetic moment as well as the Dirac moment in his studies of the relativistic effect on the neutron and proton magnetic moments in the deuteron. Breit (6,7) studied a phenomenological spin-spin interaction, relating this interaction with the well-known Majorana and Heisenberg exchange interactions. Armand Siegel (8) adapted Breit's phenomenological approach to Dirac operators to obtain an equivalent Pauli operator which allowed him to estimate the size of relativistic corrections to n-p scattering at 90 MeV. Breit (9) again used an approximately relativistic many particle Hamiltonian and studied the resulting relativistic corrections to nuclear energy levels and magnetic moments. Blatt and Weisskopf (10) have noticed that the triton and alpha particle, because of tight binding and correspondingly high kinetic energies, require relativisitic corrections to their binding energies and magnetic moments. All of this work, as can be seen, was applied to extremely light nuclei, and these early attempts to apply

relativity to the nucleus were, for the most part, ignored in ensuing work. The reason for this is simply the agreement provided by non-relativistic theories with experimental data and the fact that relativistic theories are inherently more complicated than a corresponding non-relativistic theory.

Until the EHO was formulated, there existed no soluble single-particle model of the nucleus. In this work, we shall study the energy levels and proton density of the EHO and calculate, in the first Born approximation, elastic scattering of high energy electrons from a nucleus described by EHO wave functions.

CHAPTER II

THE EHO HAMILTONIAN AND SOLUTIONS

The "Equivalent Harmonic Oscillator" (EHO), the application of which forms the basis of this work, was introduced by N. V. V. J. Swamy (11) and arises from the exact solutions of the Dirac equation when an interaction of the form

$$V = i\lambda^2 \rho_1 (\vec{\sigma}\cdot\vec{r}) \frac{\vec{\sigma}\cdot\vec{L}+1}{|\vec{\sigma}\cdot\vec{L}+1|} \tag{1}$$

is added to the free particle Hamiltonian

$$H_{fp} = \rho_3 m_0 c^2 + \rho_1 c\, \vec{\sigma}\cdot\vec{p} \tag{2}$$

The solutions of the resulting equation

$$(H_{fp} + V)\Psi_{\nu\kappa\mu} = E\ \Psi_{\nu\kappa\mu} \tag{3}$$

are four-component spinors, formed from the Pauli spinors χ^{μ}_{κ} which are the basis functions of the irreducible representation of the spin-angle group $O(3) \otimes SU(2)$ and the radial part of the solutions of the Schroedinger equation for the three-dimensional isotropic harmonic oscillator.

The Non-Relativistic Harmonic Oscillator

The non-relativistic isotropic harmonic oscillator (NRHO) is a

well-known quantum mechanical model, and the unnormalized solutions of the Schroedinger equation with a harmonic oscillator potential are given, for example, in Rechenmethoden der Quantentheorie (12):

$$\mathcal{U}_{v\ell m}(r,\theta,\varphi) = r^{\ell} e^{-\frac{1}{2}(\alpha r)^2} {}_1F_1\left(-v, \ell+\tfrac{3}{2}; \alpha^2 r^2\right) Y_{\ell}^{m}(\theta,\varphi) \qquad (4)$$

where: ${}_1F_1$ (a, c; x) is the confluent hypergeometric function (3); $Y_{\ell}^{m}(\theta,\phi)$ is the normalized spherical harmonic, defined in the Condon-Shortley phase convention (13); and α is the "oscillator parameter"

$$\alpha = \sqrt{\frac{m_0 \omega}{\hbar}}$$

The numbers v, ℓ, m are integers, and they can take on the following values:

$$\begin{aligned} v &= 0, 1, 2, 3, \ldots \\ \ell &= 0, 1, 2, 3, \ldots \\ m &= -\ell, -\ell+1, \ldots, 0, \ldots, \ell-1, \ell\ . \end{aligned} \qquad (5)$$

As is true in any spherically symmetric field, the number v is related to the number of nodes in the radial eigenfunction, and the number ℓ is related to the orbital angular momentum of the state.

Since the spherical harmonics are normalized to unity, the normalization of these solutions is carried out over the radial part only. That is, identifying

$$F_{v\ell}(r) \equiv N_{v\ell}\, r^{\ell} e^{-\frac{1}{2}\alpha^2 r^2} {}_1F_1\left(-v, \ell+\tfrac{3}{2}; \alpha^2 r^2\right) \qquad (6)$$

we require that

$$\int_0^{\infty} \left| F_{v\ell}(r) \right|^2 r^2\, dr = 1\ . \qquad (7)$$

To evaluate this integral, we first express the confluent hypergeometric function ${}_1F_1\ (a, c; x)$ in terms of the Whitaker function $M_{\kappa,\lambda}(Z)$ (14)

$$ {}_1F_1(a,c;x) = e^{\frac{1}{2}x}\, x^{-\frac{1}{2}-\mu}\, M_{\kappa,\mu}(x) \tag{8} $$

where: $\kappa = \frac{1}{2}C - a$

$\mu = \frac{1}{2}C - \frac{1}{2}$.

We can now make use of the results derived by Melvin and Swamy (15) for integrals of the form

$$ \int_0^\infty z^{\rho}\, M_{\kappa_1,\mu_1}(z)\, M_{\kappa_2,\mu_2}(z)\ dz \ . $$

When this integration is done, the normalized radial eigenfunctions of the isotropic harmonic oscillator are given by

$$ F_{v\ell}(r) = \sqrt{\frac{2\alpha^3\,\Gamma(v+\ell+\frac{3}{2})}{v!\,[\Gamma(\ell+\frac{3}{2})]^2}}\ (\alpha r)^{\ell}\, e^{-\frac{1}{2}\alpha^2 r^2}\, {}_1F_1\left(-v, \ell+\tfrac{3}{2}; \alpha^2 r^2\right) \tag{9} $$

For a non-negative parameter v, the ${}_1F_1$ becomes a polynomial in $(\alpha^2 r^2)$, consisting of v + 1 terms. Explicit expressions for $F_{v\ell}$ for v = 0,1,2 and ℓ = 0,1,2,3,4 are given in Appendix A.

The Spin-Angle Functions χ_κ^μ

Before discussing the properties of the χ_κ^μ functions, a brief explanation of the Dirac quantum number (κ) is in order. By using this one number, we simultaneously determine both ℓ and j for that particular state. The number κ, a non-zero integer, has two definitions: one for the case where $j = \ell - \frac{1}{2}$ (spin and orbital angular momentum are anti-

parallel), $\kappa = \ell$; and another for the case where $j = \ell + \frac{1}{2}$ (spin and orbital angular momentum are parallel), $\kappa = -\ell - 1$. If we take ℓ, now a function of κ, as $\ell(\kappa)$, we then define $\ell(-\kappa)$, denoted by the symbol $\bar{\ell}$, according to:

$$\begin{aligned} &\text{for } j = \ell - \tfrac{1}{2}, \quad \bar{\ell} = \ell - 1 ; \\ &\text{for } j = \ell + \tfrac{1}{2}, \quad \bar{\ell} = \ell + 1 . \end{aligned} \tag{10}$$

We also note that, in each case, $|\kappa| = j + \frac{1}{2}$, so κ is an algebraic quantity. For each κ, there will be $2|\kappa|$ values of μ which can take on the half-integral values:

$$\mu = \pm \frac{1}{2}, \pm \frac{3}{2}, \pm \frac{5}{2}, \ldots, \pm (|\kappa| - 1/2) . \tag{11}$$

The basis functions of the irreducible representation of the three-dimension rotation group O(3) are the familiar spherical harmonics

$$Y_\ell^m(\theta,\varphi) = (-1)^m \sqrt{\frac{(2\ell+1)(\ell-m)!}{4\pi\,(\ell+m)!}}\ \sin^m\theta \cdot \frac{d^m}{d(\cos\theta)^m} P_\ell(\cos\theta)\, e^{im\varphi} \tag{12}$$

Notice that we are using the Condon-Shortley phase convention, where

$$Y_\ell^{-m} = (-1)^m Y_\ell^{m*} .$$

These functions form an orthonormal set:

$$\int_0^\pi \sin\theta\, d\theta \int_0^{2\pi} d\varphi\, Y_{\ell'}^{m'*}(\theta,\varphi)\, Y_\ell^m(\theta,\varphi) = \delta_{\ell\ell'}\, \delta_{mm'} \tag{13}$$

The basis functions of the unitary unimodular group in two dimensions [SU(2)] are the two-component eigenfunctions of $\vec{\sigma} \cdot n$, $\chi_{\frac{1}{2}}^{\frac{1}{2}}$ and $\chi_{\frac{1}{2}}^{-\frac{1}{2}}$: (16,17)

$$\chi^{\frac{1}{2}}_{\frac{1}{2}} = \begin{pmatrix} \cos\frac{\theta}{2} & e^{-i\frac{\varphi}{2}} \\ \sin\frac{\theta}{2} & e^{i\frac{\varphi}{2}} \end{pmatrix} \tag{14}$$

$$\chi^{-\frac{1}{2}}_{\frac{1}{2}} = \begin{pmatrix} -\sin\frac{\theta}{2} & e^{-i\frac{\varphi}{2}} \\ \cos\frac{\theta}{2} & e^{i\frac{\varphi}{2}} \end{pmatrix} \tag{15}$$

Since the elements of the two groups O(3) and SU(2) commute, we can form the direct product group O(3) ⊗ SU(2). Using the Clebsch-Gordan theorem, we can construct the basis functions of the irreducible representation of the irreducible compounds of this direct product group:(18)

$$\chi^{\mu}_{\kappa} = \sum_{m_s}\sum_{m_\ell} C^{\ell\ \frac{1}{2}\ j}_{m_\ell\ m_s\ \mu}\ Y^{m_\ell}_{\ell}\ \chi^{m_s}_{\frac{1}{2}} \tag{16}$$

Using a coordinate system where $\hat{n}$ is chosen to lie along the Z axis, the $\chi^{m_s}_{\frac{1}{2}}$ functions take on the usual "up-spin" and "down-spin" form:

$$\chi^{\frac{1}{2}}_{\frac{1}{2}} \rightarrow \alpha = \begin{pmatrix} 1 \\ 0 \end{pmatrix} \tag{17a}$$

$$\chi^{\frac{1}{2}}_{\frac{1}{2}} \rightarrow \beta = \begin{pmatrix} 0 \\ 1 \end{pmatrix} \tag{17b}$$

In this case, the χ^{μ}_{κ} can be represented by

$$\chi_{\kappa}^{\mu} = \begin{pmatrix} C_{\mu-\frac{1}{2}\ \frac{1}{2}\ \mu}^{\ell\ \frac{1}{2}\ j} & Y_{\ell}^{\mu-\frac{1}{2}} \\ C_{\mu+\frac{1}{2}\ -\frac{1}{2}\ \mu}^{\ell\ \frac{1}{2}\ j} & Y_{\ell}^{\mu+\frac{1}{2}} \end{pmatrix} \tag{18}$$

and we can similarly define

$$\chi_{-\kappa}^{\mu} = \begin{pmatrix} C_{\mu-\frac{1}{2}\ \frac{1}{2}\ \mu}^{\bar{\ell}\ \frac{1}{2}\ j} & Y_{\bar{\ell}}^{\mu-\frac{1}{2}} \\ C_{\mu+\frac{1}{2}\ -\frac{1}{2}\ \mu}^{\bar{\ell}\ \frac{1}{2}\ j} & Y_{\bar{\ell}}^{\mu+\frac{1}{2}} \end{pmatrix} \tag{19}$$

For the case $j = \ell - \frac{1}{2}$ ($\kappa > 0$), $\kappa = \ell$ and $\bar{\ell} = \bar{\ell} - 1$. In this instance,

$$\chi_{\kappa}^{\mu} = \begin{pmatrix} -\sqrt{\frac{\ell-\mu+\frac{1}{2}}{2\ell+1}} & Y_{\ell}^{\mu-\frac{1}{2}} \\ \sqrt{\frac{\ell+\mu+\frac{1}{2}}{2\ell+1}} & Y_{\ell}^{\mu+\frac{1}{2}} \end{pmatrix} \tag{20a}$$

and

$$\chi_{-\kappa}^{\mu} = \begin{pmatrix} -\sqrt{\frac{\ell-\mu-\frac{1}{2}}{2\ell-1}} & Y_{\ell-1}^{\mu-\frac{1}{2}} \\ \sqrt{\frac{\ell+\mu-\frac{1}{2}}{2\ell-1}} & Y_{\ell-1}^{\mu+\frac{1}{2}} \end{pmatrix} \tag{20b}$$

For the opposite case, where $j = \ell + \frac{1}{2}$ ($\kappa < 0$), $\kappa = -\ell - 1$ and $\bar{\ell} = \bar{\ell} + 1$. Then

$$\chi_{\kappa}^{\mu} = \begin{pmatrix} \sqrt{\frac{\ell+\mu+\frac{1}{2}}{2\ell+1}} & Y_{\ell}^{\mu-\frac{1}{2}} \\ \sqrt{\frac{\ell-\mu+\frac{1}{2}}{2\ell+1}} & Y_{\ell}^{\mu+\frac{1}{2}} \end{pmatrix} \tag{21a}$$

and $$\chi^{\mu}_{-\kappa} = \begin{pmatrix} \sqrt{\frac{l+\mu+3/2}{2l+3}} & Y^{\mu-1/2}_{l+1} \\ \sqrt{\frac{l-\mu+3/2}{2l+3}} & Y^{\mu+1/2}_{l+1} \end{pmatrix} \tag{21b}$$

In Appendix B, we present explicit values of χ^{μ}_{κ} and $\chi^{-\kappa}_{\mu}$ for $\kappa = \pm 1, \pm 2, \pm 3, \pm 4$.

Since multiplication of these spin-angle functions by any function of r does not alter any of the group properties, we can introduce the spinors

$$|v\ \kappa\ \mu\rangle \longrightarrow \chi^{\mu}_{\kappa}\ F_{vl} \tag{22a}$$

$$|v\ -\kappa\ \mu\rangle \longrightarrow i\ \chi^{\mu}_{-\kappa}\ F_{v\bar{l}} \tag{22b}$$

which lead to the (unnormalized) eigenvectors of the EHO Hamiltonian [Equation (3)]

$$\Phi_{v\kappa\mu} = \begin{pmatrix} |v\ \kappa\ \mu\rangle \\ \frac{S_\kappa\,(E-m_0c^2)}{2\lambda\sqrt{v+|\kappa|+\frac{1}{2}}}\ |v\ -\kappa\ \mu\rangle \end{pmatrix} \tag{23}$$

The S_κ appearing in the small component is a phase factor $S_\kappa = \kappa/|\kappa|$, and $\lambda = \hbar c\ \alpha$.

The normalization of these functions is a straightforward matter, owing to the orthonormality of $|\ v\ \kappa\ \mu\ \rangle$ and $|\ v\ -\ \kappa\ \mu\ \rangle$. Requiring that

$$\int_{\text{all space}} \Psi^{\dagger}_{v\kappa\mu}\ \Psi_{v\kappa\mu}\ d\vec{r} = 1\ ,$$

we find that the normalized eigenvectors of the EHO are given by

$$\Psi_{\upsilon\kappa\mu} = \left[1 + \frac{(E - m_o c^2)^2}{4\lambda^2(\upsilon + |\kappa| + \frac{1}{2})}\right]^{-\frac{1}{2}} \begin{pmatrix} |\upsilon\ \kappa\ \mu\rangle \\ \dfrac{S_\kappa (E - m_o c^2)}{2\lambda\sqrt{\upsilon + |\kappa| + \frac{1}{2}}}\ |\upsilon\ -\kappa\ \mu\rangle \end{pmatrix} \tag{24}$$

Non-Relativistic Limit of H_{EHO}

Foldy and Wonthuysen (19) have developed an extremely useful method of determining the non-relativistic limit of a Hamiltonian

$$H = \rho_3 m_o + \mathcal{E} + \mathcal{O} \qquad (\hbar = c = 1) \tag{25}$$

where $\mathcal{E}$ is any operator which commutes with ρ_3 (called an "even" operator) and $\mathcal{O}$ is any operator which anticommutes with ρ_3 (called an "odd" operator.) The non-relativistic limit of this Hamiltonian is, correct to order $1/m_o^2$, given by

$$H_{NR} = \rho_3 m_o + \mathcal{E} + \frac{1}{2m_o}\rho_3 \mathcal{O}^2 - \frac{1}{8m_o^2}\left[\mathcal{O}, \left[\mathcal{O}, \mathcal{E}\right]\right] \tag{26}$$

Our EHO Hamiltonian

$$H_{EHO} = \rho_3 m_o + \rho_1 \vec{\sigma}\cdot\vec{p} + i\lambda^2 \rho_1 (\vec{\sigma}\cdot\vec{r}) \frac{\vec{\sigma}\cdot\vec{L} + 1}{|\vec{\sigma}\cdot\vec{L} + 1|} \tag{27}$$

can then be written in the form of Equation (25), with

$$\mathcal{E} = 0$$

$$\mathcal{O} = \rho_1 \left\{ \vec{\sigma}\cdot\vec{p} + i\lambda^2 (\vec{\sigma}\cdot\vec{r}) \frac{\vec{\sigma}\cdot\vec{L}+1}{|\vec{\sigma}\cdot\vec{L}+1|} \right\} \tag{28}$$

Upon substitution of these expressions into Equation (26) we find, as the non-relativistic limit of the EHO Hamiltonian

$$H_{NR} = \left(1 + \tfrac{3}{2}\alpha^2 S_\kappa\right) m_o + \frac{p^2}{2m_o} + \frac{\alpha^4}{2m_o} r^2 + \left(\frac{\alpha^2}{m_o} S_\kappa\right) \vec{\sigma}\cdot\vec{L} \tag{29}$$

This is the non-relativistic Hamiltonian with a Thomas-Frenkel type of spin-orbit coupling.

Free-Particle Limit of H_{EHO}

In the Dirac description of free electrons, a "helicity operator" $(\vec{\sigma}\cdot p)$ is used a great deal (20). Roughly speaking, this describes the relation between an electron's spin and its direction of motion. (Is it spinning "right-handed" or is it spinning "left-handed?") The free-particle Dirac Hamiltonian (Equation (2)) commutes with this helicity operator, and hence the free-particle solutions $\psi_{k\kappa\mu}$ are also eigenvectors of $\vec{\sigma}\cdot p$. The free particle solutions can be written as (16)

$$\psi_\kappa^\mu = \begin{pmatrix} j_\ell(r)\, \chi_\kappa^\mu \\ \frac{\vec{\sigma}\cdot\vec{p}}{E+m_o} \left[j_\ell(r)\, \chi_\kappa^\mu \right] \end{pmatrix} \tag{30}$$

and the spherical Bessel functions $j_\ell(r)$ obey the relations

$$\left(\frac{d}{dx} - \frac{\ell}{x}\right) j_\ell(x) = - j_{\ell+1}(x) \tag{31a}$$

$$\left(\frac{d}{dx} + \frac{\ell+1}{x}\right) j_\ell(x) = j_{\ell-1}(x) \tag{31b}$$

We now show that, by defining an "oscillator helicity operator" $\vec{\sigma} \cdot \vec{b}$, a similar behavior is obeyed by the EHO eigenvectors. We define the operator

$$\vec{\sigma}\cdot\vec{b} = \vec{\sigma}\cdot\vec{p} + i\lambda^2(\vec{\sigma}\cdot\vec{r})\frac{(\vec{\sigma}\cdot\vec{L}+1)}{|\vec{\sigma}\cdot\vec{L}+1|} \tag{32}$$

Recall that the spin-angle functions obey the following relations:

$$(\vec{\sigma}\cdot\vec{L}+1)\,\chi^{\mu}_{\kappa} = -\kappa\,\chi^{\mu}_{\kappa} \tag{33}$$

$$\left(\frac{\vec{\sigma}\cdot\vec{r}}{r}\right)\chi^{\mu}_{\kappa} = -\chi^{\mu}_{-\kappa} \tag{34}$$

and the radial eigenfucntions follow the ladder operators

$$\left[\left(\frac{d}{dr}+\frac{1}{r}\right) + \frac{\ell}{r} + \lambda^2 r\right] F_{v\ell}(r) = 2\lambda\sqrt{v+\ell+\tfrac{1}{2}}\; F_{v\,\ell-1}(r) \tag{35a}$$

$$\left[\left(\frac{d}{dr}+\frac{1}{r}\right) - \frac{\ell+1}{r} - \lambda^2 r\right] F_{v\ell}(r) = -2\lambda\sqrt{v+\ell+\tfrac{3}{2}}\; F_{v\,\ell+1}(r) \tag{35b}$$

Using the fact that $\vec{\sigma}\cdot\vec{p}$ has a representation

$$\vec{\sigma}\cdot\vec{p} = -i\,\vec{\sigma}\cdot\hat{r}\left[\left(\frac{d}{dr}+\frac{1}{r}\right) - \frac{1}{r}(\vec{\sigma}\cdot\vec{L}+1)\right] \tag{36}$$

along with Equations (33 - 35b), it is a straightforward matter to show that

$$\vec{\sigma}\cdot\vec{b}\ \ |\upsilon\ \kappa\ \mu\rangle = 2\lambda S_\kappa \sqrt{\upsilon+|\kappa|+\tfrac{1}{2}}\ \ |\upsilon\ -\kappa\ \mu\rangle \tag{37a}$$

$$\vec{\sigma}\cdot\vec{b}\ \ |\upsilon\ -\kappa\ \mu\rangle = 2\lambda S_\kappa \sqrt{\upsilon+|\kappa|+\tfrac{1}{2}}\ \ |\upsilon\ \kappa\ \mu\rangle \tag{37b}$$

Using these two results, we can now write $\Phi_{\upsilon\kappa\mu}$ in a simple, elegant form:

$$\Phi_{\upsilon\kappa\mu} = \begin{pmatrix} |\upsilon\ \kappa\ \mu\rangle \\ \dfrac{\vec{\sigma}\cdot\vec{b}}{E+m_o}\ |\upsilon\ \kappa\ \mu\rangle \end{pmatrix} \tag{38}$$

and the formal resemblance to the free-particle eigenvectors [Equation (30)] is obvious, since we recall that

$$|\upsilon\ \kappa\ \mu\rangle = F_{\upsilon\ell}(r)\ \chi^{\mu}_{\kappa}\ . \tag{22a}$$

The spin-angle part of both vectors are identical (χ^{μ}_{κ}). If we identify a k_{HO} and drop any term in λ^2 or higher, Equations (37a) and (37b) reduce to

$$\left[\left(\frac{d}{dr}+\frac{1}{r}\right)+\frac{\ell}{r}\right] F_{\upsilon\ell}(r) \longrightarrow k_{HO}\ F_{\upsilon\ \ell-1}(r) \tag{39a}$$

$$\left[\frac{d}{dr}-\frac{\ell}{r}\right]\ F_{\upsilon\ell}(r) \longrightarrow k_{HO}\ F_{\upsilon\ \ell+1}(r) \tag{39b}$$

while the spherical Bessel fcns (the radial part of the free-particle

solution) satisfy

$$\left[\left(\frac{d}{dr}+\frac{1}{r}\right)+\frac{l}{r}\right] j_l(k_{fp}\,r) \rightarrow k_{fp}\; j_{l-1}(k_{fp}\,r) \qquad (40a)$$

$$\left[\frac{d}{dr}-\frac{l}{r}\right] j_l(k_{fp}\,r) \longrightarrow k_{fp}\; j_{l+1}(k_{fp}\,r) \qquad (40b)$$

The correspondence between the EHO and free-particle radial wave functions is now easily seen.

Thus, in the free-particle limit of the EHO ($\lambda \rightarrow 0$), the EHO Hamiltonian [Equation (27)] reduces directly to the free-particle Hamiltonian [Equation (2)]; the angular part of the eigenvectors are identical to the free-particle case, and the radial part of the vectors obey a similar set of ladder operators as the spherical Bessel functions.

Relation of the EHO to the Nilsson Hamiltonian

S. G. Nilsson (21) proposed a non-relativistic model of the nucleus, based on the isotropic harmonic oscillator. Beginning with the Schroedinger Hamiltonian H_o of the spherically symmetric harmonic oscialltor, he added angular momentum-dependent terms $C\vec{\ell}\cdot\vec{s}$ and $D\vec{\ell}^2$, obtaining

$$H_o = \overset{o}{H}_o + C\vec{\ell}\cdot\vec{s} + D\vec{\ell}^2 .$$

Finally, adding a deformation term H_δ which is related to the nucleus' quadrupole moment, the Nilsson Hamiltonian is found to be

$$H = \overset{o}{H}_o + C\vec{\ell}\cdot\vec{s} + D\vec{\ell}^2 + H_\delta ,$$

where

$$H_\delta = -\delta\, h\, \omega_o \frac{4}{3}\sqrt{\frac{\pi}{5}}\; r^2\, Y_2^o .$$

The correspondence between this term and the quadrupole moment can be seen by Equation VIII.1 of reference (22), where the quadrupole moment is defined by

$$Q = \frac{1}{e} \int r^2 (3\cos^2\theta - 1)\, \rho(r)\, d\vec{r}$$

Since

$$Y_2^0 = \sqrt{\frac{5}{16\pi}}\ (3\cos^2\theta - 1)$$

we find that the deformation of the nucleus as represented by Nilsson's H_δ is directly related to the quadrupole moment. We now wish to examine the EHO Hamiltonian

$$H_{EHO} = \rho_3 m_0 + \rho_1 \vec{\sigma}\cdot\vec{p} + i\lambda^2 \rho_1 \vec{\sigma}\cdot\vec{r}\ \frac{\vec{\sigma}\cdot\vec{L}+1}{|\vec{\sigma}\cdot\vec{L}+1|} \qquad (27)$$

and see if a possible correspondence can be made with the Nilsson Hamiltonian, perhaps through the non-relativistic approximation. If we want to add any terms to the EHO Hamiltonian, we will require that the new Hamiltonian have the same set of eigenvectors. Since

$$\left[H_{EHO},\ \rho_3 (\vec{\sigma}\cdot\vec{L}+1) \right] = 0$$

such a term is a possible addition.

It is interesting to note that if we add a term

$$\varepsilon \rho_3 (\vec{\sigma}\cdot\vec{L} + 1)$$

to the EHO Hamiltonian (Equation (27)), the same set of eigenvectors are obtained, and the only effect of this term is to displace the energy levels by $-\varepsilon\kappa$. Since this is an even operator in the Dirac sense, we can obtain an approximate non-relativistic limit of

$$H' = H_{EHO} + \varepsilon \rho_3 (\vec{\sigma}\cdot\vec{L} + 1)$$

by iterating the Hamiltonian H'. When this is done, we can make a one-to-one correspondence with the terms in the non-relativistic limit of H_{EHO} with those in the Nilsson Hamiltonian:

$$k^2_{REL} \rightarrow k^2_{NR}$$

$$\lambda^4 r^2 \rightarrow m_o^2 \omega^2 r^2$$

$$\varepsilon^2 \vec{L}^2 \rightarrow 2m_o D \vec{\ell}^2$$

$$(2\lambda^2 S_\kappa + \varepsilon^2 + 2\varepsilon m_o)\vec{\sigma}\cdot\vec{L} \rightarrow 2m_o C \vec{\ell}\cdot\vec{s}$$

$$i\varepsilon [(\vec{\sigma}\cdot\vec{L} + 1), (\vec{\sigma}\cdot\vec{b})] \rightarrow 2m_o H_\delta,$$

and we have scaled the EHO energy levels to remove a constant term.

CHAPTER III

THE EHO AS A NUCLEAR SHELL MODEL

In this chapter, we discuss how the EHO Hamiltonian can be used as a model of the nucleus. To begin with, ours will be an extreme single-particle model. That is, each nucleon is assumed to move in an average potential (described by the EHO interaction) independent of the motion of the other nucleons. Also, since our Hamiltonian is charge independent, no difference will be seen between the proton states and the neutron states.

The energy of the single particle state described by the quantum numbers (v, κ, μ) was seen to be

$$E_{EHO} = \sqrt{m_0^2 c^4 + 4\lambda^2 (v + |\kappa| + \tfrac{1}{2})} \tag{38}$$

As we have seen, the EHO is intimately connected with the NRHO, and it is interesting to compare the energy levels of the EHO with those of the NRHO. Flügge (12), among others, has given the NRHO energy levels as

$$E_{NRHO} = (2v + l + \tfrac{3}{2}) \hbar\omega \tag{39}$$

As shown in Table I, the degeneracy of the EHO is exactly four times that of the NRHO. Note, however, that when the NRHO is applied to a system of Fermions, two particles (protons) are allowed per state, so that the degeneracy then becomes twice that shown in Table I. The EHO states, being solutions of the Dirac equation, already contain spin and

the Pauli exclusion principle allows only one particle per EHO state.

TABLE I

DEGENERACY OF THE EHO AND THE NRHO

EHO			NRHO		
$E^2 - m_o^2c^4$	$v + \lvert\kappa\rvert$	Degeneracy	E	$2v + \ell$	Degeneracy
$6\lambda^2$	1	4	$\frac{3}{2}\hbar\omega$	0	1
$10\lambda^2$	2	12	$\frac{5}{2}\hbar\omega$	1	3
$14\lambda^2$	3	24	$\frac{7}{2}\hbar\omega$	2	6
$18\lambda^2$	4	40	$\frac{9}{2}\hbar\omega$	3	10
$22\lambda^2$	5	60	$\frac{11}{2}\hbar\omega$	4	15
$26\lambda^2$	6	84	$\frac{13}{2}\hbar\omega$	5	21

Since we have this degeneracy between a great number of states, we are at liberty to fill the states within any energy level in any order we choose. One of the criteria should be, of course, to use as consistent and logical a scheme as possible, consistent with experimental data. We also do not want to split any of the $2|\kappa|$ μ-degenerate states for any given κ unless we add a perturbation to our Hamiltonian. Consequently, we feel free to rearrange the order in which the κ states are filled. Ultimately, one must make a compromise between a systematic scheme which may not agree with experimental data and a phenomenological ordering which fits the data but provides little insight into the problem.

As in atomic physics, the primary clue to the order in which succeeding states are filled is provided by the binding energy of the last

particle added. In both atomic and nuclear physics, certain numbers of particles are particularly stable, resulting in the so-called "magic" and "semi-magic" numbers. For nuclei, the following numbers of protons have been found to be especially stable (22)

$$Z = 2, 8, 20, 28, 50, 82, 126 .$$

In addition to these, nuclei with Z = 14 and Z = 40 are relatively stable, though not as pronounced as the others. We would then like a scheme which allows these numbers to be identified with the least amount of splitting. In Table II, we present four possible schemes for filling the states.

The first scheme presented (column I) follows the general ordering used in the Mayer-Jensen shell model (22) with no spin-orbit coupling, and this ordering allows only three magic numbers (Z = 2, 8, 28) and the two semi-magic numbers (Z = 14, 40) without splitting a κ state into its $2|\kappa|$ substates.

The second scheme (column II) is based on the shell model also, but here we have added the effect of a hypothetical spin-orbit interaction which depresses the energy of the $\kappa = -1$ state for each v, such that it is the first κ value filled in each energy level. This decrease in the energy of the positive κ state relative to the negative κ is a known consequence of an $\vec{\ell} \cdot \vec{s}$ interaction, but our assumption that it affects only the $|\kappa| = 1$ states is completely arbitrary, as is our estimate of the magnitude of the splitting. Accepting this as our model, though, we find that we still have three magic numbers (Z = 2, 50, 82) and the two semimagic numbers available with no splitting of a κ into its substates.

The third scheme presented (column III) is a completely arbitrary

ordering, chosen solely because all the magic numbers (Z = 2, 8, 20, 28, 50, 82, 126) and the semimagic numbers (Z = 14, 40) are allowed. However, it does show that all these numbers can be accommodated without hypothesizing any perturbation which will split the $2|\kappa|$ degenerate μ-states. That is, all the magic and semimagic numbers can be found without splitting any of the κ states.

The last one shown (column IV) is the order we chose for most of our work. (The exception is $_2He^4$, and this is discussed later.) In this scheme, we simply fill the states with lowest angular momentum first, working up to the highest ℓ ($|\kappa|$) values. Using this simple scheme, we find all but two of the magic numbers: Z = 2, 8, 20, 28, 82. In addition, the semimagic number Z = 40 appears.

In each of these four methods, we have followed the practice of filling the $j = \ell + \frac{1}{2}$ state (negative κ) before the $j = \ell - \frac{1}{2}$ (positive κ) state, as predicted by the NRHO with spin-orbit coupling (22). Since this is precisely the non-relativistic limit of the EHO, it seems reasonable that we should use this ordering.

TABLE II

$E^2 - m_o^2c^4$	Column I			Column II				Column III				Column IV			
	v	κ	Z	v	κ	Z		v	κ	Z		v	κ	Z	
$22\ \lambda^2$	4	1	140	4	1	140		3	2	140		0	5	140	
	4	-1	138	3	2	138		3	-2	136		0	-5	130	
	3	2	136	3	-2	134		2	3	132		1	4	120	
	3	-2	132	2	3	130		2	-3	126	(126)	1	-4	112	
	2	3	128	2	-3	124		1	4	120		2	3	124	
	2	-3	122	1	4	118		1	-4	112		2	-3	98	
	1	4	116	1	-4	110		0	5	104		3	2	92	
	1	-4	108	0	5	102		0	-5	94		3	-2	88	
	0	5	100	0	-5	92		4	1	84		4	1	84	
	0	-5	90	4	-1	82	(82)	4	-1	82	(82)	4	-1	82	(82)
$18\ \lambda^2$	3	1	80	3	1	80		0	4	80		0	4	80	
	3	-1	78	2	2	78		0	-4	72		0	-4	72	
	2	2	76	2	-2	74		1	3	64		1	3	64	
	2	-2	72	1	3	70		1	-3	58		1	-3	58	
	1	3	68	1	-3	64		3	1	52		2	2	52	
	1	-3	62	0	4	58		3	-1	50	(50)	2	-2	48	
	0	4	56	0	-4	50	(50)	2	2	48		3	1	44	
	0	-4	48	3	-1	42		2	-2	44		3	-1	42	

TABLE II (Continued)

$E^2 - m_o{}^2c^4$	Column I				Column II				Column III				Column IV			
	v	κ	Z		v	κ	Z		v	κ	Z		v	κ	Z	
$14\,\lambda^2$	2	1	40	(40)	2	1	40	(40)	0	3	40	(40)	0	3	40	(40)
	2	-1	38		1	2	38		0	-3	34		0	-3	34	
	1	2	36		1	-2	34		1	2	28	(28)	1	2	28	(28)
	1	-2	32		0	3	30		1	-2	24		1	-2	24	
	0	3	28	(28)	0	-3	24		2	1	20	(20)	2	1	20	(20)
	0	-3	22		2	-1	18		2	-1	18		2	-1	18	
$10\,\lambda^2$	1	1	16		1	1	16		1	1	16		0	2	16	
	1	-1	14	(14)	0	2	14	(14)	1	-1	14	(14)	0	-2	12	
	0	2	12		0	-2	10		0	2	12		1	1	8	(8)
	0	-2	8	(8)	1	-1	6		0	-2	8	(8)	1	-1	6	
$6\,\lambda^2$	0	1	4		0	1	4		0	1	4		0	1	4	
	0	-1	2	(2)	0	-1	2	(2)	0	-1	2	(2)	0	-1	2	(2)

CHAPTER IV

COMPARISON OF THE EHO WITH EXPERIMENT

An important aspect of any nuclear model is the distribution of particles in the nucleus. From a knowledge of the spatial distribution of the nucleons, it is possible to derive many properties of nuclear structure such as the total angular momentum, the multipole moments, and the differential cross-sections for electron scattering. In our work, we are concerned entirely with the predictions of the EHO for the electron scattering cross-sections.

Radial Density of the EHO

Since we will later use the Born approximation with a spherically symmetric charge distribution, we will need the radial density $\rho(r)$, defined by

$$\rho(r) = \frac{\int_0^{2\pi} d\varphi \int_0^{\pi} \sin\theta \, d\theta \; \psi^* \psi}{\int_0^{2\pi} d\varphi \int_0^{\pi} \sin\theta \; d\theta} \tag{40}$$

or, equivalently,

$$\rho(r) = \frac{1}{4\pi} \int_0^{2\pi} d\varphi \int_0^{\pi} \sin\theta \; d\theta \;\; \psi^* \psi \; . \tag{41}$$

Notice that, since ψ is normalized to unity,

$$4\pi \int_0^\infty \rho(r)\, r^2\, dr = 1 \tag{42}$$

For the NRHO,

$$\psi(r,\theta,\varphi) = F_{v\ell}(r)\, Y_\ell^m(\theta,\varphi) \tag{43}$$

Since the Y_ℓ^m's are orthonormal, we obtain the simple (and useful) result:

$$\rho_{v\ell}(r) = \frac{1}{4\pi} \left| F_{v\ell}(r) \right|^2 \tag{44}$$

The EHO densities are not as simple, since the EHO vectors are four-component functions. In evaluating $\rho(r)$ for the EHO, we first perform a matrix multiplication between the four-row column vector $|\Psi_{v\kappa\mu}>$ and the four-column row vector $<\Psi_{v\kappa\mu}|$. Having taken this scalar product, the integration over the angles is performed, and we find that the radial density of the EHO state $\Psi_{v\kappa\mu}$ is given by

$$\rho_{v\kappa}(r) = \left[1 + \frac{(E - m_0c^2)^2}{4\lambda^2 (v + |\kappa| + \frac{1}{2})} \right]^{-1} \left[\rho_{v\ell}(r) + \frac{(E - m_0c^2)^2}{4\lambda^2 (v + |\kappa| + \frac{1}{2})}\, \rho_{v\bar{\ell}}(r) \right] \tag{45}$$

where $\rho_{v\ell}(r)$ and $\rho_{v\bar{\ell}}(r)$ are the corresponding NRHO densities. Thus, the EHO density can be expressed as the sum of two NRHO densities, involving ℓ and $\ell \pm 1$. We might note here that both $\rho_{v\ell}(r)$ and $\rho_{v\kappa}(r)$ are in closed form, expressed as the sum of a series of Gaussian terms.

Since ours is an extreme independent particle model, the total nuclear density will simply be the sum of the single-particle densities over the first Z states. (To keep the nuclear density normalized to

unity, we divide by Z).

$$\rho_Z(r) = \frac{1}{Z} \sum_{i=1}^{Z} \rho_{v_i \kappa_i}(r) \tag{46}$$

and

$$4\pi \int_0^\infty \rho_z(r)\, r^2 dr = 1 . \tag{47}$$

Although ρ_z can, in principle, be evaluated without recourse to numerical computation, the algebra involved in calculating ρ_z for, say, lead or indium becomes very laborious. It was therefore decided to utilize the digital computer in this work. A program was written in the Fortran IV language of the IBM 360/50 which begins with Kummer's Series for the confluent hypergeometric function (14):

$$_1F_1(a,c;x) = 1 + \frac{a}{c}\frac{x}{1!} + \frac{a(a+1)}{c(c+1)}\frac{x^2}{2!} + \frac{a(a+1)(a+2)}{c(c+1)(c+2)}\frac{x^3}{3!} + \cdots \tag{48}$$

and calculates the coefficients a_n in the expressions for the normalized radial densities of both the single particle states of the NRHO and the total nuclear densities of the EHO and NRHO. This program is described in Appendix C, and provides the a_n in the following expression:

$$\rho(r) = \alpha^3 \sum_n a_n (\alpha r)^{2n} e^{-\alpha^2 r^2} \tag{49}$$

In Table III, we list the coefficients in the total nuclear density for the NRHO and the EHO for five selected nuclei. In the case of EHO helium, two densities are presented: one for the case where the two $\kappa = -1$ states are filled, the other for the case where the two $\kappa = 1$ states are filled. As mentioned earlier, there seems to be some ambigu-

TABLE III

COEFFICIENTS IN THE DENSITIES OF SELECTED NUCLEI

$_2He^4$:	NRHO:	a_1	= .17960
	EHO:	a_1	= .024329
		a_2	= .10351
$_6C^{12}$:	NRHO:	a_1	= .05986
		a_2	= .07981
	EHO:	a_1	= .074595
		a_2	= .103665
		a_3	= -.06017
		a_4	= .013344
$_{20}Ca^{40}$:	NRHO:	a_1	= .044897
		a_2	= 0
		a_3	= .0359174
	EHO:	a_1	= .07857
		a_2	= -.007483
		a_3	= .02634
		a_4	= -.0071835
		a_5	= .00068414
$_{49}In^{115}$:	NRHO:	a_1	= .018325
		a_2	= .03665
		a_3	= -.01466
		a_4	= .009773
		a_5	= .0005585
	EHO:	a_1	= .048104
		a_2	= .03207
		a_3	= -.031888
		a_4	= .02036

TABLE III (Continued)

		a_5	= -.002452
		a_6	= .0002125
		a_7	= .0000429
		a_8	= .000006449
$_{82}Pb^{208}$:	NRHO:	a_1	= .01916
		a_2	= 0
		a_3	= .03066
		a_4	= -.01168
		a_5	= .00292
		a_6	= .0000809
	EHO:	a_1	= .030183
		a_2	= .03433
		a_3	= -.06284
		a_4	= .09033
		a_5	= -.05448
		a_6	= .01848
		a_7	= -.0035111
		a_8	= .0003778
		a_9	= -.00002101
		a_{10}	= .0000004868

ity in filling the states in helium, so we have presented both configurations in Table III. This question will be considered more carefully when we look at the plot of $\rho(r)$ vs. r (Figure 1).

Determination of the Oscillator Parameter

As indicated, the densities involve one adjustable parameter, the oscillator constant α $(=\sqrt{m_o\omega/\hbar})$. To determine this parameter, there are several possibilities. One which was considered was to calculate the theoretical expressions for the quadrupole moment Q and to equate this to the experimentally observed values of Q. This approach was rejected, however, because a second parameter occurs in the expression for Q--the depth of the potential well. Since this is another arbitrary feature of a harmonic oscillator model, we chose instead a comparison between root-mean-square (r.m.s.) radii.

The r.m.s. radius (squared) is simply the expectation value of r^2 in the state $\Psi_{\nu\kappa\mu}$:

$$a^2_{\nu\kappa} \equiv \langle r^2 \rangle_{\nu\kappa} \equiv \langle \Psi_{\nu\kappa\mu} \mid r^2 \mid \Psi_{\nu\kappa\mu} \rangle \tag{50}$$

The r.m.s. radius of the total nucleus (consisting of Z protons) is simply the average of the individual single-particle radii:

$$a^2_Z = \frac{1}{Z} \sum_{i=1}^{Z} \langle r^2 \rangle_{\nu_i\kappa_i} \tag{51}$$

For the EHO, the expectation value of r^2 is a complicated function of α, so that when we sum up Z of these expressions and take the average, it becomes necessary to solve an implicit integral equation to extract

α. A simpler, if somewhat less precise, method is to compare the NRHO expression for α with experiment and use this value of α in the corresponding EHO densities, and this is the method chosen to find α. As an estimate of the error involved in this procedure, we consider the case of $_{20}Ca^{40}$, a closed-shell nucleus in the EHO model. For closed-shell nuclei, we can extract a simple expression for α from the EHO as well. Equating this expression with experimental data (12), we find $\alpha = .539\ F^{-1}$, while the NRHO comparison yields $\alpha = .492\ F^{-1}$. Thus, using the simpler NRHO expression, our value of α is approximately 10% smaller than the proper EHO value. Our primary concern in this study is the comparison of predicted cross-sections with observed cross-sections, so the significance of this 10% difference lies in its effect on $d\sigma/d\Omega$. The cross-sections for $\alpha = .539$ and $\alpha = .492$ in the case of 757.5-MeV scattering from Ca^{40} was calculated and compared with the experimental results reported by Bellicard (24). The 10% decrease in α resulted in a shift of the diffraction minimum toward smaller angles by an amount 6^{o}. Although this is not negligible, the basic agreement (or more precisely, disagreement) between theory and experiment was not materially affected. For this reason, we feel justified in using the more accessible values of α predicted by the NRHO.

The expectation value of r^2 for the NRHO is easily calculated by use of Equation (8), and is given by the expression

$$a^2_{vl} = \alpha^{-2}\,(2v + l + 3/2) \tag{52}$$

The average r.m.s. radius for the nucleus is then

$$a^2_Z = \frac{1}{Z}\sum_{i=1}^{Z}(2v_i + l_i + 3/2) \tag{53}$$

and we can equate this expression to experimentally determined values of a, thereby fixing the value of the oscillator parameter α.

Review of Experimental Work in Elastic Scattering of Electrons

Nearly every experimental group studying nuclear structure has calculated a r.m.s. radius appropriate to an assumed theoretical model. Of the many techniques used, we shall confine ourselves to a review of work done in high energy elastic scattering of electrons, since it is through these experiments that the most direct information regarding nuclear densities can be obtained. For electrons of 150 MeV, the deBroglie wavelength is approximately 8 F. Since the nuclear radius is roughly 5 F, we can expect high energy electrons to reflect the shape and density of the nucleus to the extent that the scattering is dependent on the distribution of protons in the nucleus.

Robert Hofstadter has presented a definitive review of the experimental work done in this field prior to 1957 in his two review articles (25, 26). In reference (26), he has given a table listing the important parameters (including the r.m.s. radius) for the accepted nuclear models for 22 different nuclei, and references are made to the previous work done for these nuclei. In this introduction we shall confine our attention to work that has been done since 1957 in the field of high energy elastic scattering of electrons. The following references are listed chronologically, according to the date of publication.

Ravenhall (27) summarizes work done by his group for four nuclei. For scattering of 400 MeV electrons from He^4, the r.m.s. radius (a) was calculated to be 1.61 F for a Gaussian shape. For 187 MeV scattering

from C^{12}, a = 2.40 F for a harmonic oscillator model. For 420 MeV scattering from Au^{197}, the r.m.s. radii are the same as those reported by Hofstadter (25). Ehrenberg (28) disagreed with the radii reported in (27), stating that they were generally too small. Ehrenberg has given the cross-sections for scattering from O^{16} and C^{12} for the following incident energies: E_o = 240 MeV, 360 MeV, and 420 MeV. For a parabolic well, the r.m.s. radius of C^{12} is a = 2.50 F, and for O^{16}, a = 2.70 F.

Ulrich Meyer-Berkhout and others (29) studied nuclei of the 1p shell (Be^9, B^{10}, B^{11}, N^{14}, O^{16}) with energies between 160 MeV and 420 MeV. In their Table IV (16, p. 146), the parameters for several of the common models of these nuclei are reported. Burleson and Kendall (30) used a Gaussian model of the He^4 nucleus with a = 1.68 F in their analysis of 302 MeV electron scattering. Crannell et al. (31) studied 183 MeV scattering from Ca^{40}, V^{51}, Co^{59}, In^{115}, $Sb^{121,123}$, and Bi^{209}, using a Fermi distribution with "C" parameters C = 3.64, 3.92, 4.10, 5.25, 5.37, 6.49 F respectively. (For the Fermi distribution, C represents the distance from the center of the nucleus to the point where the radial density reaches one-half its central value.)

In their study of radiative transition widths in excited states of carbon, Crannell and Griffy (32) measured the cross-sections for elastic scattering of 250 MeV electrons from the C^{12} nucleus. In their analysis, they used a harmonic oscillator density with r.m.s. radius a = 2.43 F. In a different approach, Goldemberg (33) varied the incident energy and measured the cross-section for elastic scattering at 180^o only. For B^{10} and B^{11}, Goldemberg calculated the oscillator parameter to be α = .646 F^{-1}.

Repellin, et al. (34) disagreed with Hofstadter's (25) choice of

the Gaussian distribution for He^4, and proposed that the form factor be given instead by the expression

$$F(q) = (1 - 0.101\ q^2)\ \exp\ (-\ 0.29\ q^2)\ .$$

About a year after this paper was published, Frosch et al. (35) defended Hofstadter's original choice, claiming that a = 1.643 F for He^4. Frank and co-workers (36) also measured the charge radius of the helium nucleus, reporting that a = 1.63 F for the α-particle.

Applying a Fermi three parameter (also called a parabolic Fermi) density to their results for 250 MeV scattering from Ca^{40}, Croissaux (37) determined a to be 3.52 F. Also, for the first time, two diffraction minima were observed. The effect of the neutrons on the charge distribution was studied by Van Oostrum (38) in his investigation of the isotope effect in Ca^{40}, Ca^{44} and Ca^{48} through elastic scattering of 250 MeV electrons. Although the addition of the extra neutrons increased the size of nucleus according to the familiar $A^{1/3}$ law, the charge density at the edge (r ~ 4F) was found to be greater for Ca^{40} than for Ca^{48}.

Crannell (39) gave the cross-sections for scattering of 600 MeV and 800 MeV electrons from C^{12} and O^{16}. For C^{12}, a = 2.40 F, while for O^{16}, a = 2.65 F. By observing scattering at 175 MeV and 250 MeV, Bellicard and van Oostrum (40) determined the "half-density parameter" C [see reference (31)] to be C = 6.47 F. By adding a small undulation to the parabolic Fermi shape, Bellicard et al. (24) were able to obtain excellent agreement with the cross-sections observed for scattering of 757.5 MeV electrons from Ca^{40} and Ca^{48}. Here, a second and third diffraction minimum was observed. The C parameter used had the value C = 3.7369 F. Frosch et al. (41) studied electron scattering from He^4 nuclei at several

energies with the most complete data reported for 800 MeV. For a Fermi three-parameter shape, a r.m.s. radius of a = 1.71 F was used. In a later paper (42), Frosch et al. studied scattering of 250 MeV electrons from $Ca^{40,42,44,48}$ and Ti^{48}, and 500 MeV scattering from $Ca^{40,48}$. The r.m.s. radius for the three-parameter Fermi shape is reported for all of these isotopes, and for Ca^{40}, a = 3.487 F. Again, a second diffraction minimum was observed.

In a theoretical paper, Donnelly and Walker (43) used the unpublished results of McCarthy and Sick for electron scattering from C^{12} and O^{16}. For each of these, a harmonic oscillator shape was used, and for C^{12} the oscillator parameter used is given by $\alpha = .610\ F^{-1}$. For O^{16}, $\alpha = .565\ F^{-1}$. In their analysis of 250 MeV and 400 MeV scattering, Dally et al. (44) report a r.m.s. radius for N^{15} of a = 2.7 F for the Fermi shape and 2.6 F for the shell model. Using the same sort of a shape as that of Bellicard (38) (parabolic Fermi with a small undulation), Heisenberg (45) was able to fit the observed cross-sections for 248 MeV and 502 MeV scattering from Pb^{208} using a r.m.s. radius of a = 5.501 F. Studying lower energy scattering from Pb^{208} and Bi^{209} (incident energies between 40 MeV and 60 MeV), Van Niftrik (46) determined the r.m.s. radii for Pb^{208} and Bi^{209} to be a = 5.46 F and 5.48, respectively. Finally, Singhal et al. (47) determined the r.m.s. radius of O^{16} to be a = 2.70 F in their studies of the isotope effect in $O^{16,17,18}$.

Giving a more general discussion, two monographs can be mentioned here. Robert Hofstadter (48), in his 1963 collection of reprints Nuclear and Nucleon Structure, has compiled approximately 50 articles, many of which have been listed above. These articles deal with both

experimental data and theoretical interpretation of the results, and, like Elton's 1961 monograph Nuclear Sizes (49), considers other experimental approaches (e.g., α-particle scattering, scattering of muonic atoms, etc.).

Radial Densities

For the main body of this present work, we have chosen five nuclei to study in some detail: He^4, C^{12}, Ca^{40}, In^{115}, and Pb^{208}. These particular isotopes were chosen to cover the range of light nuclei, medium nuclei and heavy nuclei, and because a fair amount of experimental data is available for each. Some preliminary work was also done on O^{16}, Co^{59} and Bi^{209}, but this work is not discussed here. Since there is obviously a variance in the reported r.m.s. radii for each nucleus, the best we can do is to choose the value that seems to be the most reliable. Once a value for a is chosen, we can substitute this a into Equation (53) and solve for the oscillator parameter α. Our choices for a and the corresponding oscillator parameter are given in Table IV.

TABLE IV

OSCILLATOR PARAMETERS FOR THE NUCLEI UNDER STUDY

Nucleus	a(F)	Reference	Oscillator Parameter (F^{-1})
He^4	1.71	(29)	0.716
C^{12}	2.41	(26)	0.611
Ca^{40}	3.52	(12)	0.492
In^{115}	4.50	(12)	0.448
Pb^{208}	5.501	(33)	0.371

By substituting these values of α in Equation (53), along with the coefficients given in Table III, we can plot $\rho(r)$ as a function of r and compare the radial densities predicted by the EHO and NRNO with the phenomenological shapes reported in the literature. The phenomenological shapes chosen are given below in Table IV.

In Figures (1), (2), (3), (4), and (5) are presented the radial density according to the EHO, the NRHO, and these phenomenological shapes.

In Figure 1, we have given the EHO density for two configurations: Curve I is for the two $\kappa = -1$ states being occupied, and curve IV is for the two $\kappa = +1$ states being occupied. The scheme we have generally used [column IV of Table II] fills the $\kappa = -1$ states. However, as we noted in the introduction to this paper, evidence exists (10) that, for He^4 at least, it is the $\kappa = +1$ states that are occupied. Hence, we include the density of both configurations for helium, and we can see that the EHO for the $\kappa = +1$ states (curve IV) is very similar to the phenomenological shape (curve III).

In Figure 2, the EHO predicts a more sharply peaked density than either of the other two choices. The close similarity between curves I and III is to be expected, since each is drawn for the harmonic oscillator density. The difference is due to the fact that our oscillator parameter ($a = .611\ F^{-1}$) was chosen by matching the r.m.s. radii, while Ehrenberg's oscillator parameter ($\alpha = .606\ F^{-1}$) was chosen to match the location of the diffraction minimum in the electron cross-sections.

Figures 3 and 4 show clearly the higher central density of the EHO as compared with either the Fermi or NRHO densities for Ca^{40} and In^{115}.

Figure 5 shows the same sort of behavior, but here we notice that

TABLE V

PHENOMENOLOGICAL DENSITIES

Nucleus	Reference	Name of Model	Density	Normalization Constant
He^4	(41)	Fermi Three-Parameter	$\rho = \frac{(1 + .43799\ r^2)}{1 + \exp\ (3.0581\ r - 3.08256)}$	N = 1/16.8
C^{12}	(28)	Harmonic Oscillator	$\rho = (1 + .489745\ r^2)\ \exp\ (-r^2/2.7225)$	N = 1/75.0
Ca^{40}	(42)	Fermi Three-Parameter	$\rho = \frac{(1 - .007556\ r^2)}{1 + \exp\ (r/.5839 - 6.28275)}$	N = 1/233.5
In^{115}	(25)	Fermi Uniform	$\rho = \frac{1}{1 + \exp\ (r/.5227 - 10.02487)}$	N = 1/661.8
Pb^{208}	(45)	Fermi Three-Parameter (ignoring a small undulation)	$\rho = \frac{(1 + .0085048)}{1 + \exp\ (r^2/8.3417 - 4.76286)}$	N = 1/1378.5

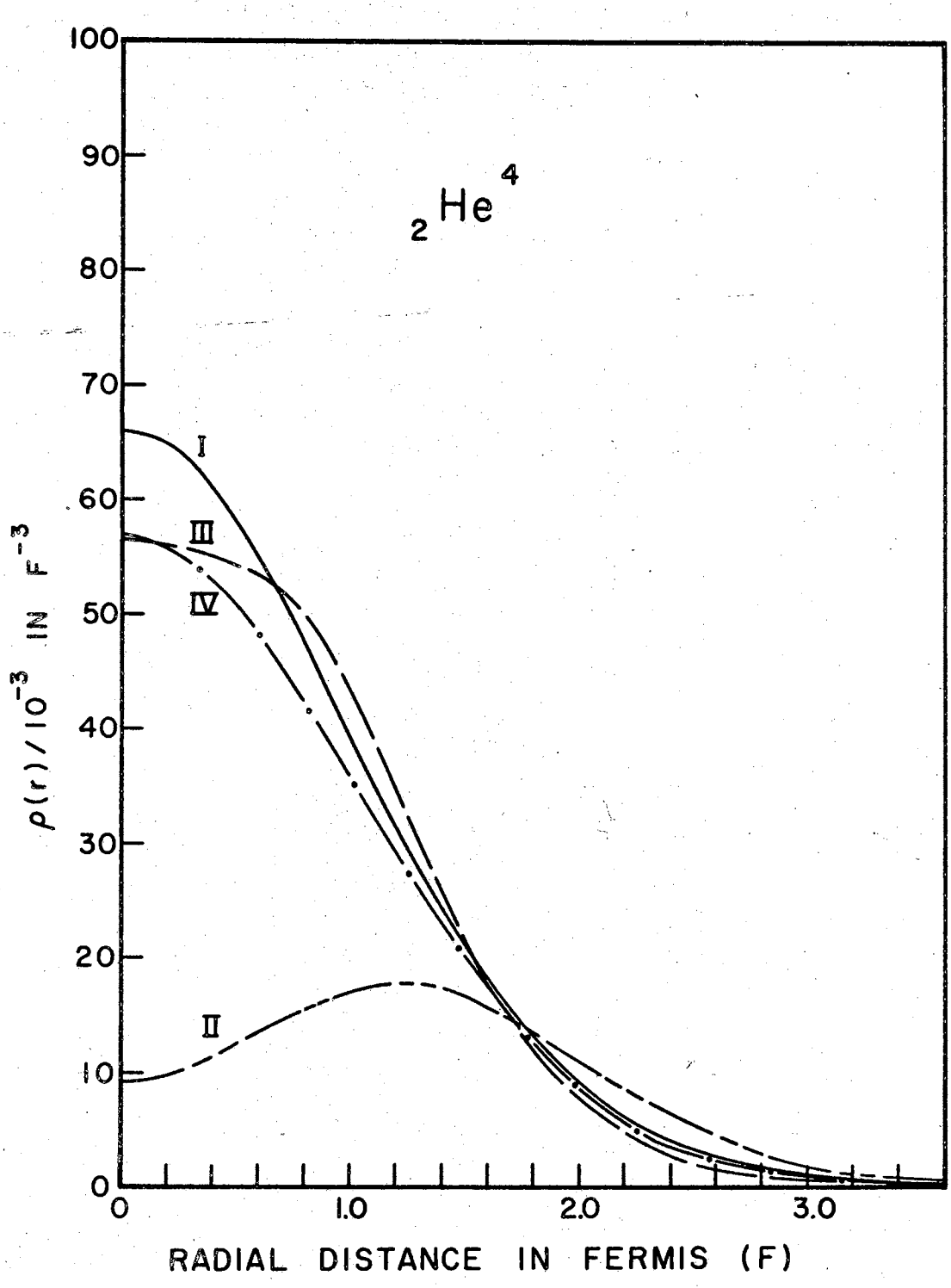

Figure 1. Proton Density in He^4. Curve I shows the NRHO density. Curve II shows the EHO density with the $\kappa = -1$ states filled. Curve III is the Fermi three-parameter shape (41), and curve IV is the EHO with the $\kappa = +1$ states filled.

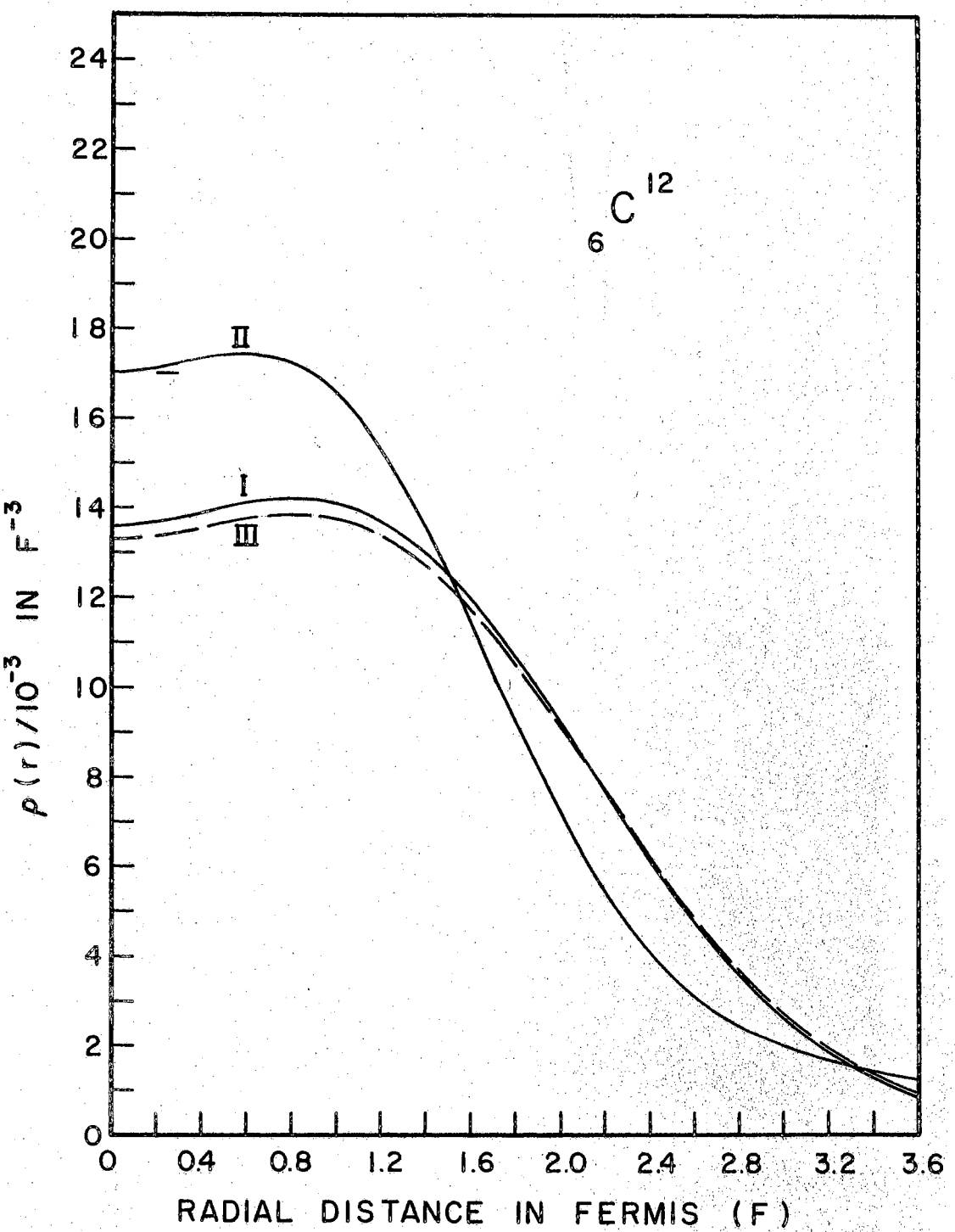

Figure 2. Proton Density in C^{12}. Curve I is the NRHO, curve II is the EHO density, and curve III is the harmonic oscillator density chosen by Ehrenberg (28).

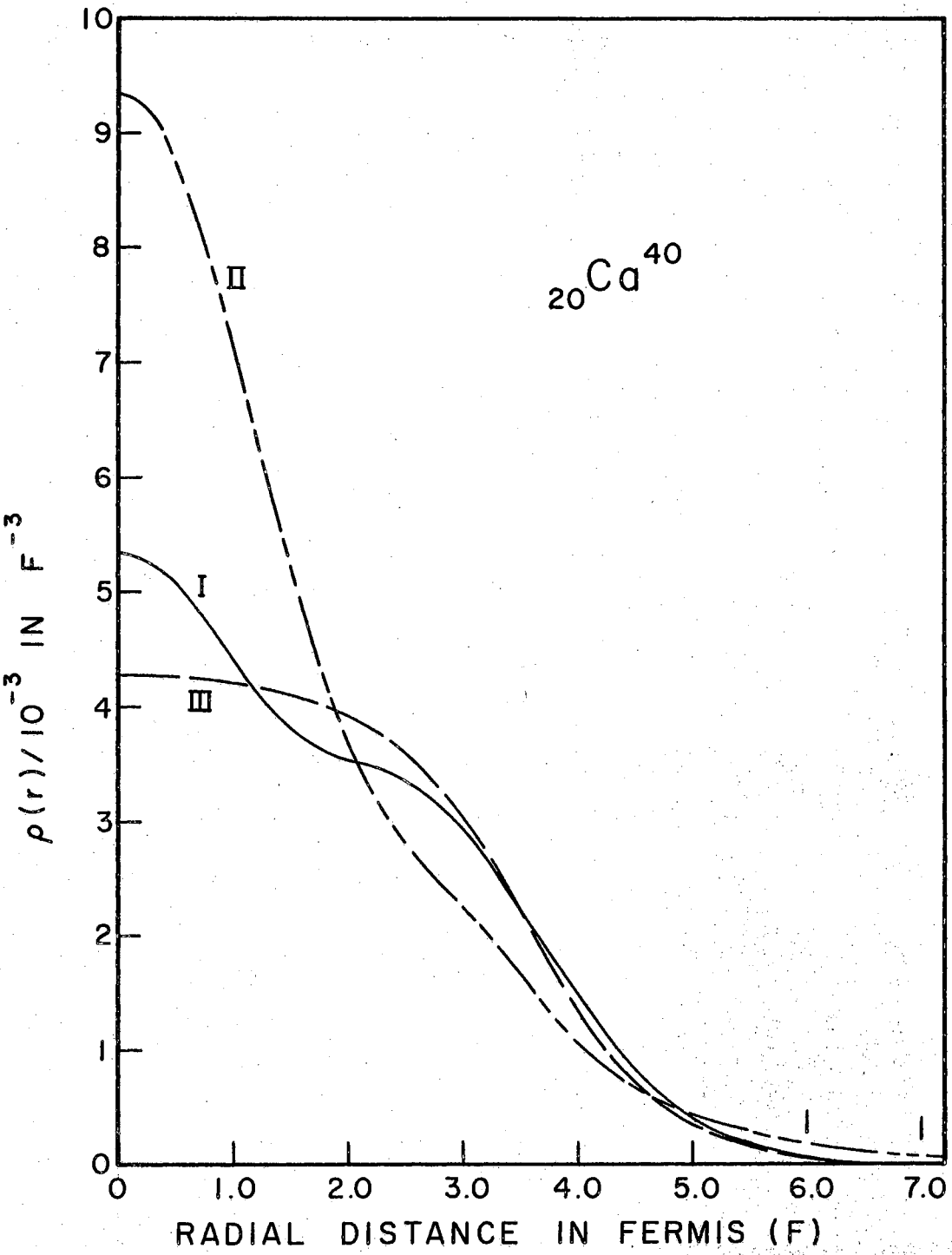

Figure 3. Proton density in Ca^{40}. Curve I is the NRHO density, curve II is the EHO density, and curve III is the Fermi three-parameter shape of reference (42).

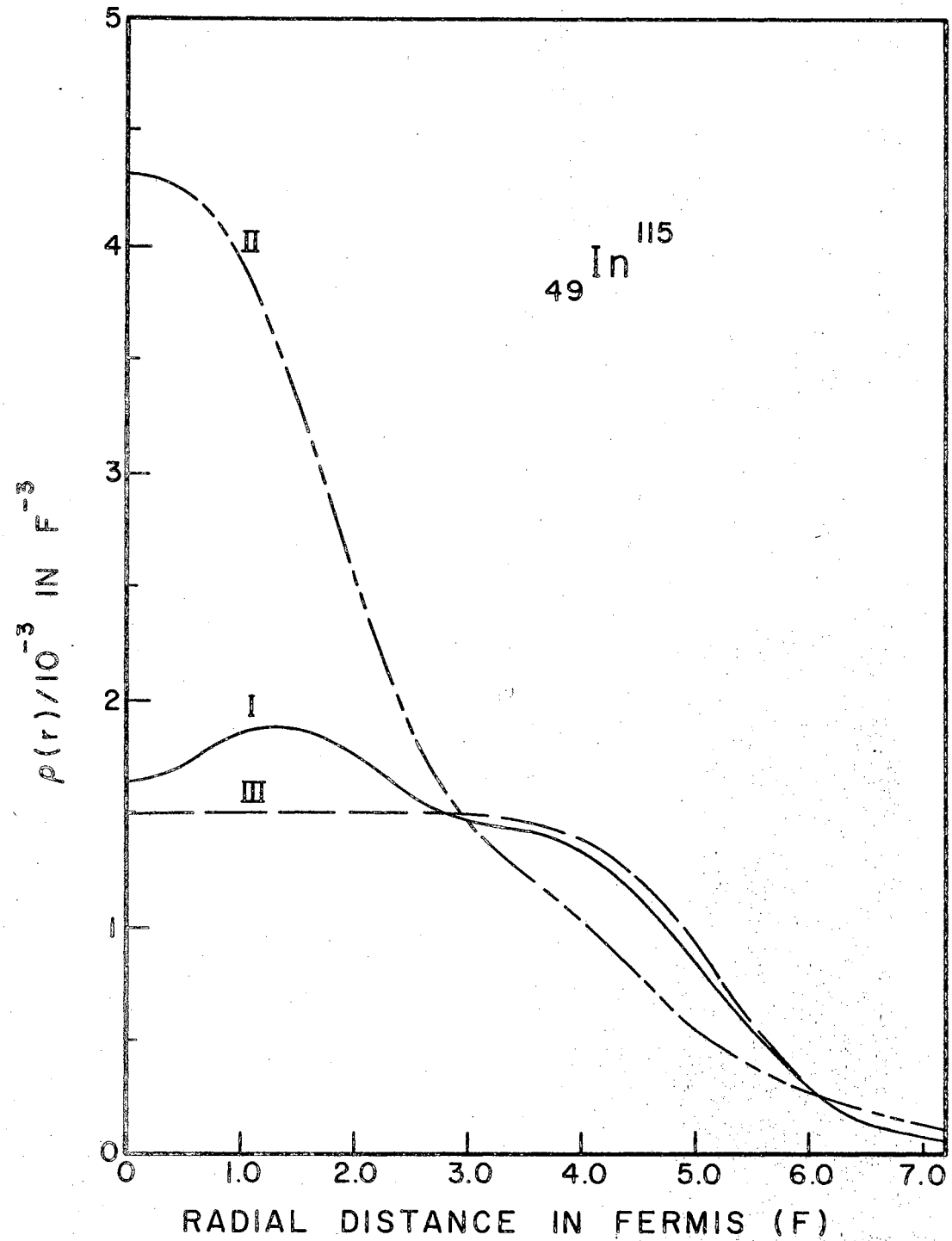

Figure 4. Proton Density in In^{115}. Curve I is the NRHO density, curve II is the EHO density, and curve III is the Fermi uniform model used in reference (25).

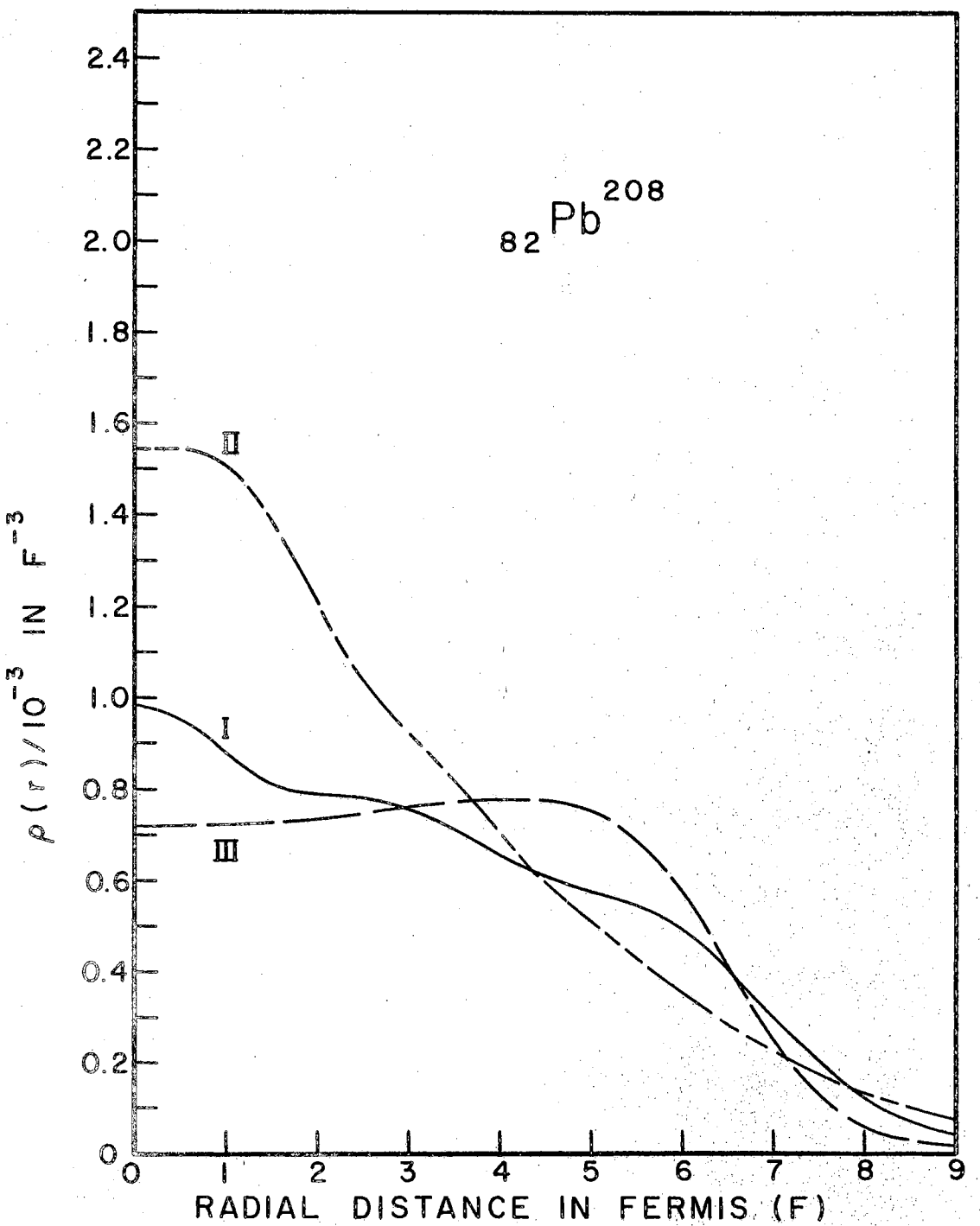

Figure 5. Proton Density in Pb^{208}. Curve I is the NRHO density, curve II is the EHO density, and curve III is the Fermi three-parameter shape of reference (45).

the phenomenological shape actually shows a central depression rather than the usual peak.

In every case but helium, we notice that the EHO predicts a more sharply peaked density than any of the non-relativistic models used. This could perhaps be caused by a tighter binding due to large kinetic energies involved in relativistic motion.

Theory of Electron Scattering

The most direct information regarding the distribution of protons in the nucleus comes from elastic scattering of electrons and measurement of the angular distribution of the scattered electrons.

The differential cross-section is the ratio of the intensity of the beam scattered into a solid angle $d\Omega$ $[I(\Omega)]$ to the intensity of the incident beam I_o:

$$\frac{d\sigma}{d\Omega} = \frac{I(\Omega)}{I_o} \tag{54}$$

The connection between this quantity and the structure was first pointed out by Rose (50), and a development of the related equations is given in Schweber (51), Schiff (52, 53) and Smith (54).

Let us define a coordinate system where $\vec{r}$ is the position of the electron and $\vec{R}$ is the coordinate of a volume element $d\vec{R}$ in the nucleus. Then, at large distances, we can write the (plane wave) wavefunctions of the electron as:

$$\psi_i(\vec{r},t) = u(\vec{p}_i)\, e^{i(\vec{p}_i\cdot\vec{r} - E_i t)} \tag{55}$$

$$\psi_f(\vec{r},t) = u(\vec{p}_f)\, e^{i(\vec{p}_f\cdot\vec{r} - E_f t)} \tag{56}$$

where ψ_i represents the incoming particle, ψ_f represents the outgoing particle (i → initial, f → final); $u(\vec{p})$ is the Dirac spinor for the electron. Also, units of $c = \hbar = 1$ are used throughout this derivation, and the center of mass coordinate system is used.

The probability of a transition from state $|i\rangle = \psi_i$ to state $|f\rangle = \psi_f$ is given by the "Second Golden Rule of Quantum Mechanics:"

$$w = \frac{2\pi}{\hbar} \left| \langle f | V | i \rangle \right|^2 \frac{dn}{dE} \tag{57}$$

where $\frac{dn}{dE}$ is the density of accessible final states, and V is the interaction causing the transition. In elastic Coulomb (non-radiative) scattering, $E_f = E_i \equiv E_o$, and $V = Ze^2/r$, so

$$w_{i \to f} = 2\pi \left| u(\vec{p}_f)^\dagger \frac{4\pi Z e^2}{|\vec{p}_f - \vec{p}_i|^2} \gamma^0 u(\vec{p}_i) \right|^2 \tag{58}$$

represents the probability per unit time that a transition will occur from the initial state $|i\rangle$ to the final state $|f\rangle$. Since we are interested in scattering of an unpolarized beam of electrons, we average over the (two) initial states. Also, since we only look at the total number of particles scattered into solid angle $d\Omega$ without regard to spin states, we sum over all possible final states. This can be expressed as the trace of a product matrix, as shown:

$$w_{total} = \frac{(2\pi)^3}{|\vec{p}_f - \vec{p}_i|^4} \cdot 4Z^2e^4 \cdot \frac{1}{2} \mathrm{Tr} \left\{ \frac{\not{p}_f + m}{m} \gamma^0 \frac{\not{p}_i + m}{m} \gamma^0 \right\} \frac{dn}{dE} \tag{59}$$

The trace can be shown to be

$$\frac{1}{2}\,\mathrm{Tr}\{\quad\} = \frac{E^2}{m^2}\left(1 - v^2 \sin^2\frac{\theta}{2}\right) \tag{60}$$

and, in an elastic scattering process, $|\vec{p}_i| = |\vec{p}_f| \equiv p$:

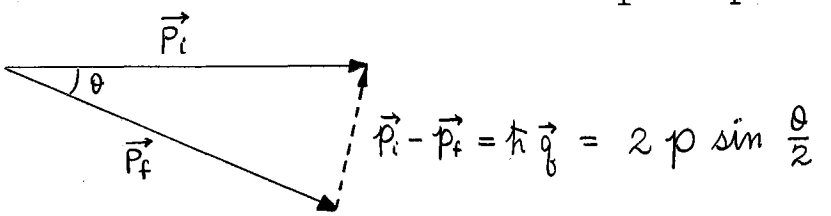

Since $\frac{dn}{dE} = \frac{mp}{(2\pi)^3}\,d\Omega$ and $\frac{d\sigma}{d\Omega} = \frac{w}{v} = \frac{w}{p/m}$

$$\frac{d\sigma}{d\Omega} = \frac{Z^2 e^4}{4p^2 v^2}\left(\frac{1 - v^2\sin^2\frac{\theta}{2}}{\sin^4\frac{\theta}{2}}\right) \tag{61}$$

In the high-energy region (E_o > 100 MeV), $1 - v^2\sin^2\frac{\theta}{2} \to \cos^2\frac{\theta}{2}$, we therefore find that the differential cross-section for the scattering of high-energy Dirac particles (spin ½) from a point nucleus is given by the Mott formula: (55, 56)

$$\frac{d\sigma}{d\Omega} = \left(\frac{Ze^2}{2E}\right)^2\left(\frac{\cos^2\frac{\theta}{2}}{\sin^4\frac{\theta}{2}}\right) \tag{62}$$

To allow for the finite size of the nucleus, we express the differential cross-section as

$$\frac{d\sigma}{d\Omega} = \frac{1}{v}\cdot\frac{1}{2}\sum_i\sum_f \frac{2\pi}{\hbar}\left|\langle f|V|i\rangle\right|^2\frac{dn}{dE} \tag{63}$$

If the nucleus is not a point mass,

$$V = -\sum_{j=1}^{Z} \frac{Ze^2}{|\vec{r} - \vec{R}_j|} \tag{64}$$

where $\vec{R}_j$ is the position vector of the $j^{\underline{th}}$ proton. Substitution of Equation (64) into Equation (63) gives

$$\frac{d\sigma}{d\Omega} = \frac{E^2 e^2 \cos^2 \frac{\theta}{2}}{c^4} \sum_{j=1}^{Z} \iint \varphi^{\dagger}(\vec{R}_j)\, \varphi(\vec{R}_j) \frac{1}{|\vec{r} - \vec{R}_j|} e^{i(\vec{q}\cdot\vec{r})}\, d\vec{r}\, d\vec{R}_j \tag{65}$$

where $(\vec{R}_j)$ is the wave function of the $j^{\underline{th}}$ proton in the nucleus. We can now expand the two terms in the integrand:

$$\frac{1}{|\vec{r} - \vec{R}_j|} = 4\pi \sum_{\ell=0}^{\infty} \sum_{m=-\ell}^{\ell} \frac{1}{2\ell+1} \frac{R_j^{\ell}}{r^{\ell+1}} Y_{\ell}^{m*}(\Theta, \Phi)\, Y_{\ell}^{m}(\theta, \varphi) \tag{66}$$

$$e^{i\vec{q}\cdot\vec{r}} = 4\pi \sum_{\ell=0}^{\infty} i^{\ell} j_{\ell}(qr) \sum_{m=-\ell}^{\ell} Y_{\ell}^{m*}(\theta, \varphi)\, Y_{\ell}^{m}(\theta, \varphi) \tag{67}$$

Substitution of Equations (66) and (67) into Equation (65) enables us to integrate over the electron coordinates only, leaving

$$\frac{d\sigma}{d\Omega} = \left(\frac{Ze^2}{2E}\right)^2 \frac{\cos^2 \frac{\theta}{2}}{\sin^4 \frac{\theta}{2}} \left| \int \varphi^{\dagger}(\vec{R})\, \varphi(\vec{R})\, e^{i\vec{q}\cdot\vec{R}}\, d\vec{R} \right|^2 \tag{68}$$

Keeping only the $\ell = 0$ term in the expansion for $e^{i\vec{q}\cdot\vec{R}}$ (monopole transitions only), we find

$$\frac{d\sigma}{d\Omega} = \left(\frac{Ze^2}{2E}\right)^2 \left(\frac{\cos^2\frac{\theta}{2}}{\sin^4\frac{\theta}{2}}\right) \left|F(q)\right|^2 \tag{69}$$

where we have identified the "nuclear form factor:"

$$F(q) = \frac{4\pi}{q}\int_0^\infty \rho(R)\ \sin(qR)\ R\,dR \tag{70}$$

Recall that these quantities are all derived in the center-of-mass coordinate system. The transformation to the lab frame gives us the results

$$q = \left(\frac{2E_0}{\hbar c}\right) \frac{\sin\frac{\theta}{2}}{\sqrt{1 + (2E_0/Mc^2)\sin^2(\theta/2)}} \tag{71}$$

$$F(q) = \frac{4\pi}{q}\int_0^\infty \rho(r)\ \sin(qr)\ r\,dr \tag{72}$$

$$\frac{d\sigma}{d\Omega} = \left(\frac{Ze^2}{2E_0}\right)^2 \left[\frac{\cos^2(\theta/2)}{\sin^4(\theta/2)}\right] \left[\frac{\left|F(q)\right|^2}{1 + (2E_0/Mc^2)\sin^2(\theta/2)}\right] \tag{73}$$

The calculation of these quantities, especially $\frac{d\sigma}{d\Omega}$, now becomes the central problem in our work, since we now have a direct comparison between theory [$\rho(r)$] and experiment [$I(\theta)/I_o$]. In general, evaluation of the integral in Equation (72) must be done numerically, because of the complicated structure of $\rho(r)$. However, for radial densities like those of the EHO and the NRHO, it is possible to evaluate this integral in closed form. Recall that our radial densities (Equation 49) can be

expressed as a series of Gaussian terms. The Laplace transform

$$\int_0^\infty e^{-pt}\, t^{\nu} \sin(2\beta^{\frac{1}{2}} t^{\frac{1}{2}})\, dt =$$

$$(-1)^{\nu} 2^{-\nu-\frac{1}{2}} \pi^{\frac{1}{2}} p^{-\nu-1} e^{-\frac{\beta}{p}} He_{2\nu+1}(2^{\frac{1}{2}} \beta^{\frac{1}{2}} t^{\frac{1}{2}}) \qquad (74)$$

has been evaluated in the literature (reference (23), Equation 4.7 (33),) so we can express the form factor of the NRHO and EHO densities as a series of terms involving the Hermite polynomials. Expressing $He_n(x)$ in terms of the more common Hermite polynomials by use of (57)

$$He_n(x) = 2^{-\frac{1}{2}n} H_n(2^{-\frac{1}{2}} x) \qquad (75)$$

we can express the Hermite polynomial itself in closed form by use of

$$H_n(x) = n! \sum_m \frac{(-1)^m (2x)^{n-2m}}{m!\,(n-2m)!} \qquad (76)$$

Successively using Equations (74), (75), and (76) in the expression for F(q), we find that, for a radial density given by

$$\rho(r) = e^{-\alpha^2 r^2} \sum_{n=1}^{10} a_n \alpha^{2n+1} r^{2n-2} \qquad (77)$$

the form factor can be written exactly as

$$F(q) = e^{-q^2/4\alpha^2} \sum_{m=1}^{10} C_m (q/\alpha)^{2m-2} \qquad (78)$$

where

$$C_m = \frac{\pi^{\frac{3}{2}} (-1)^{m-1}}{(2m-1)!} \sum_{n=m}^{10} \frac{2^{-2n+2} a_n (2n-1)!}{(n-m)!} \qquad (79)$$

TABLE VI

COEFFICIENTS IN THE FORM FACTOR OF SELECTED NUCLEI

$_2He^4$:	NRHO:	c_1	= 1.0
	EHO:	c_1	= 1.0
		c_2	= - .1441
$_6C^{12}$:	NRHO:	c_1	= 1.0
		c_2	= - .111111
	EHO:	c_1	= 1.0
		c_2	= - .2131
		c_3	= .02782
		c_4	= - .001161
$_{20}Ca^{40}$:	NRHO:	c_1	= 1.0
		c_2	= - .25
		c_3	= .125
	EHO:	c_1	= 1.0
		c_2	= - .35
		c_3	= .063333
		c_4	= - .0057738
		c_5	= .00025297
		c_6	= - .0000037202
$_{49}In^{115}$:	NRHO:	c_1	= 1.0
		c_2	= - .42857
		c_3	= .04898
		c_4	= - .001725
		c_5	= .000012147
	EHO:	c_1	= 1.0
		c_2	= - .50842
		c_3	= .11966

TABLE VI (Continued)

		c_4	= - .0141933
		c_5	= .000889795
		c_6	= -2.7959×10^{-5}
		c_7	= 4.0195×10^{-7}
		c_8	= -2.19177×10^{-9}
$_{82}Pb^{208}$:	NRHO:	c_1	= 1.0
		c_2	= - .54878
		c_3	= .0884145
		c_4	= - .0052991
		c_5	= .00011191
		c_6	= -4.3994×10^{-7}
	EHO:	c_1	= 1.0
		c_2	= - .60519
		c_3	= .157077
		c_4	= - .022375
		c_5	= .00200836
		c_6	= - .00012092
		c_7	= 4.8763×10^{-6}
		c_8	= -1.23852×10^{-7}
		c_9	= 1.7518×10^{-9}
		c_{10}	= -1.0342×10^{-11}

In Table VI, we give the values of C_m for the a_n coefficients given in Table III, given by the computer program of Appendix C.

The most striking feature of the Born approximation is the existence of sharp diffraction minima in the cross-sections. This is understandable because the first Born approximation (which we have used) treats the electrons as plane waves being diffracted by a roughly spherical center giving rise to diffraction minima. The success or failure of any model ultimately depends on how accurately these minima are predicted. As we can see from Equation (73), these minima correspond to the zeros of the form factor F(q), and in our case, to the zeros of the polynomial in Equation (78). By constructing a Sturm series (58) for these polynomials (see Appendix D), we can easily find the number of zeros in any given interval. In Table VII, we give the number of zeros of the form factor F(q) in the entire possible range of q ($0 \leq q < \infty$).

TABLE VII

ZEROS OF THE FORM FACTOR

Nucleus	Number of Zeros in F(q)	
	NRHO	EHO
He^4	0	1
C^{12}	1	1
Ca^{40}	2	1
In^{115}	4	1
Pb^{208}	5	1

As we see, the EHO predicts one minimum for each of the five nuclei under study. (This is not always true, however; Co^{59}, for ex-

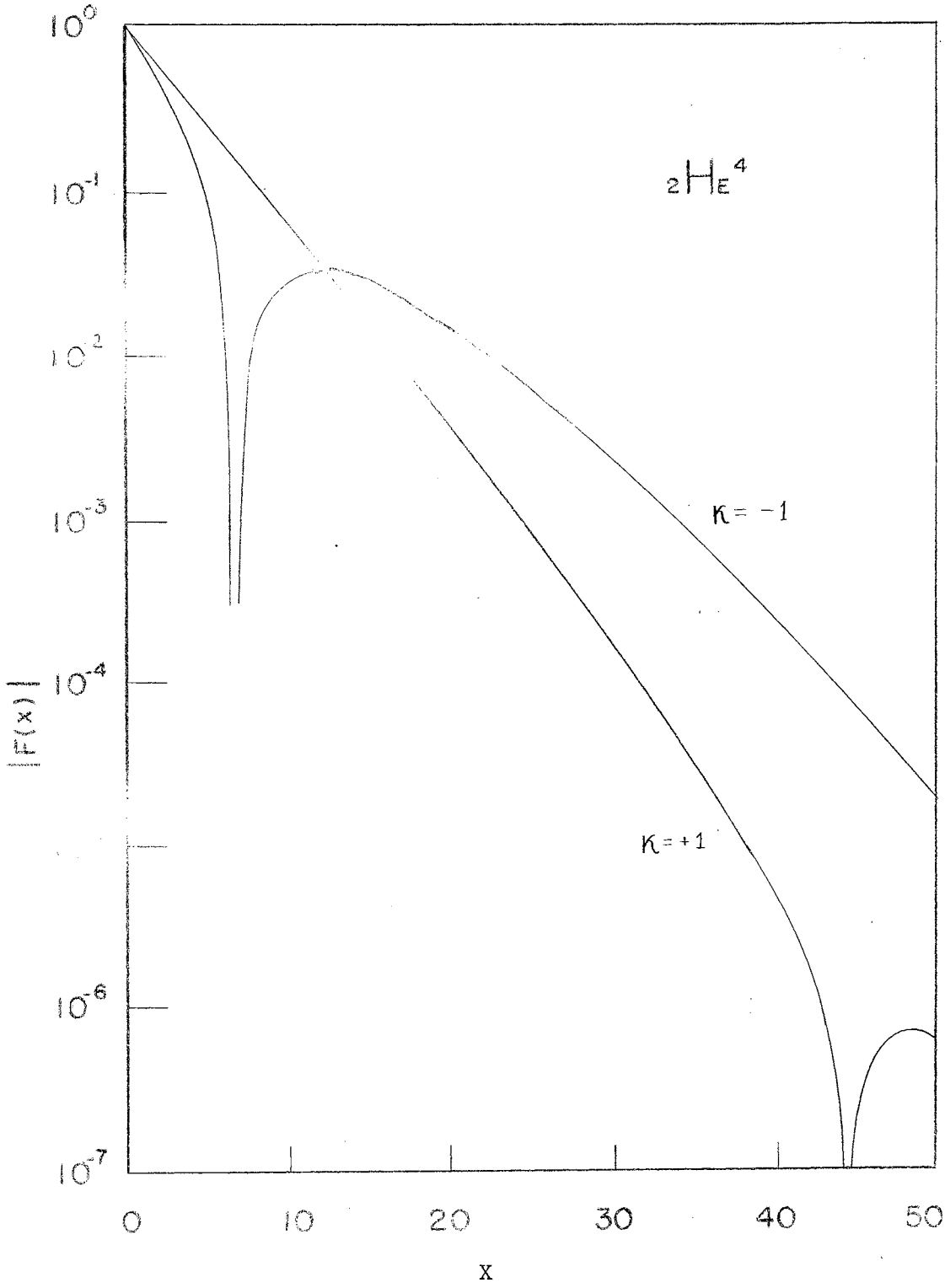

Figure 6. Absolute Value of the Form Factor for He^4

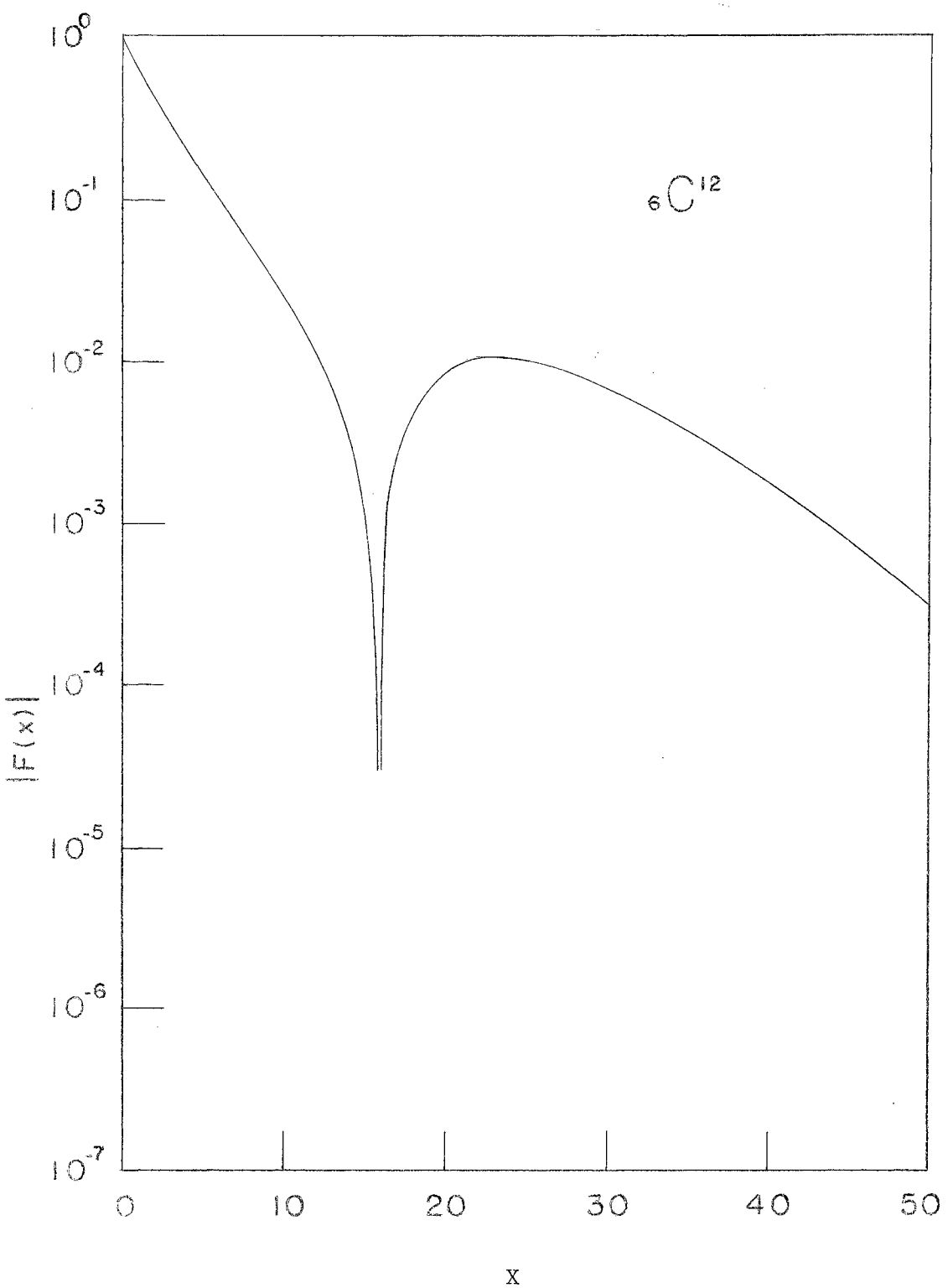

Figure 7. Absolute Value of the Form Factor for C^{12}

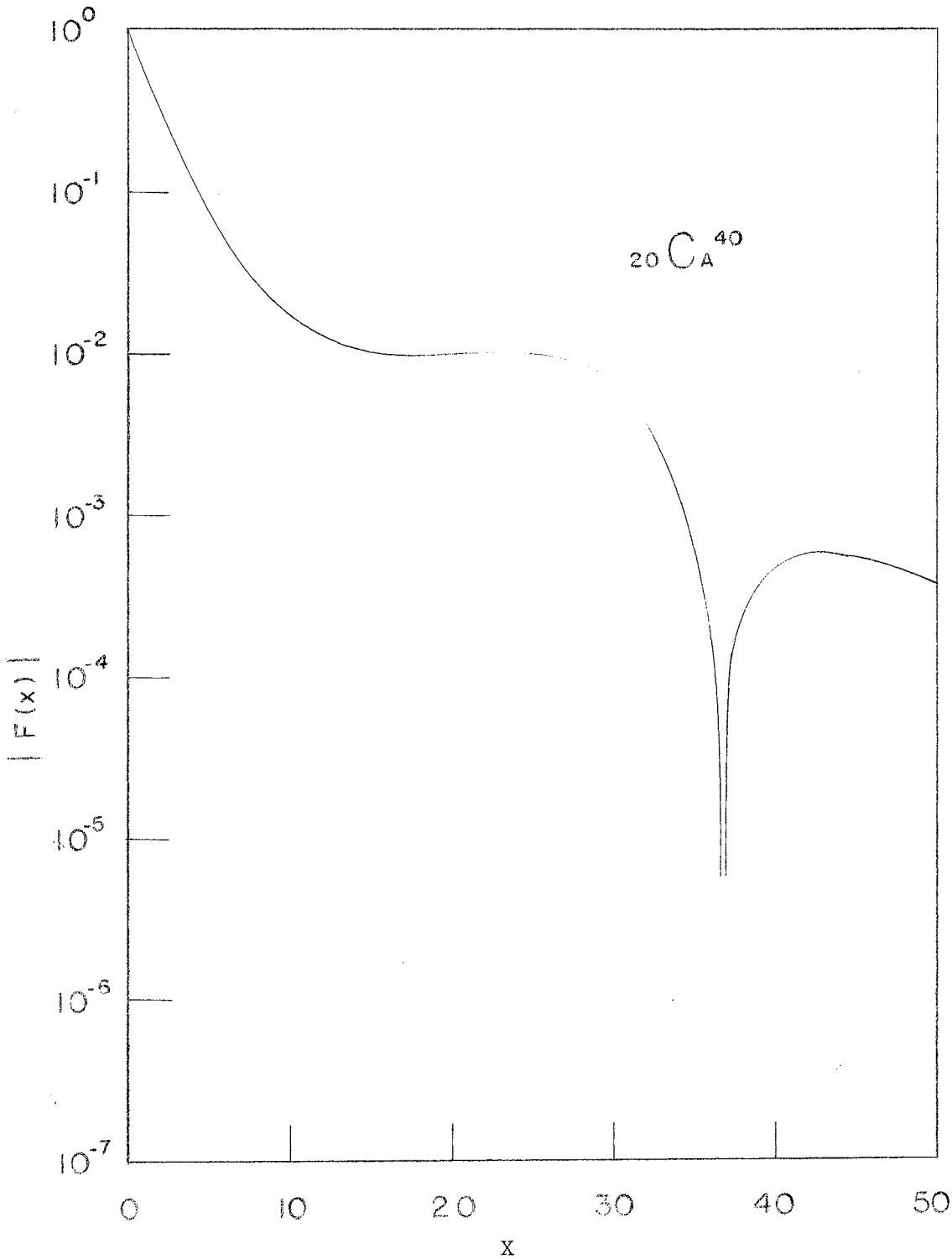

Figure 8. Absolute Value of the Form Factor for Ca^{40}

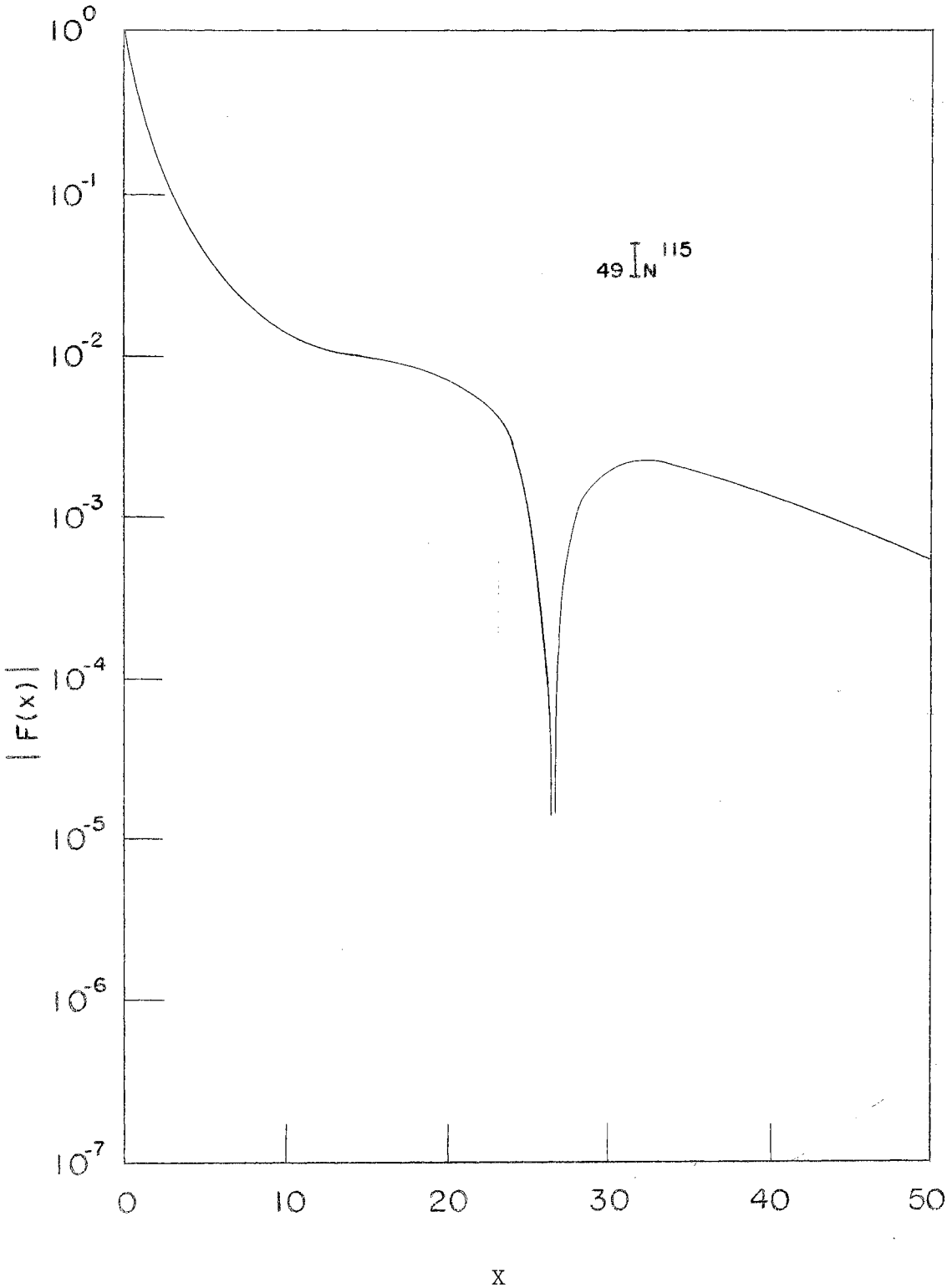

Figure 9. Absolute Value of the Form Factor for In^{115}

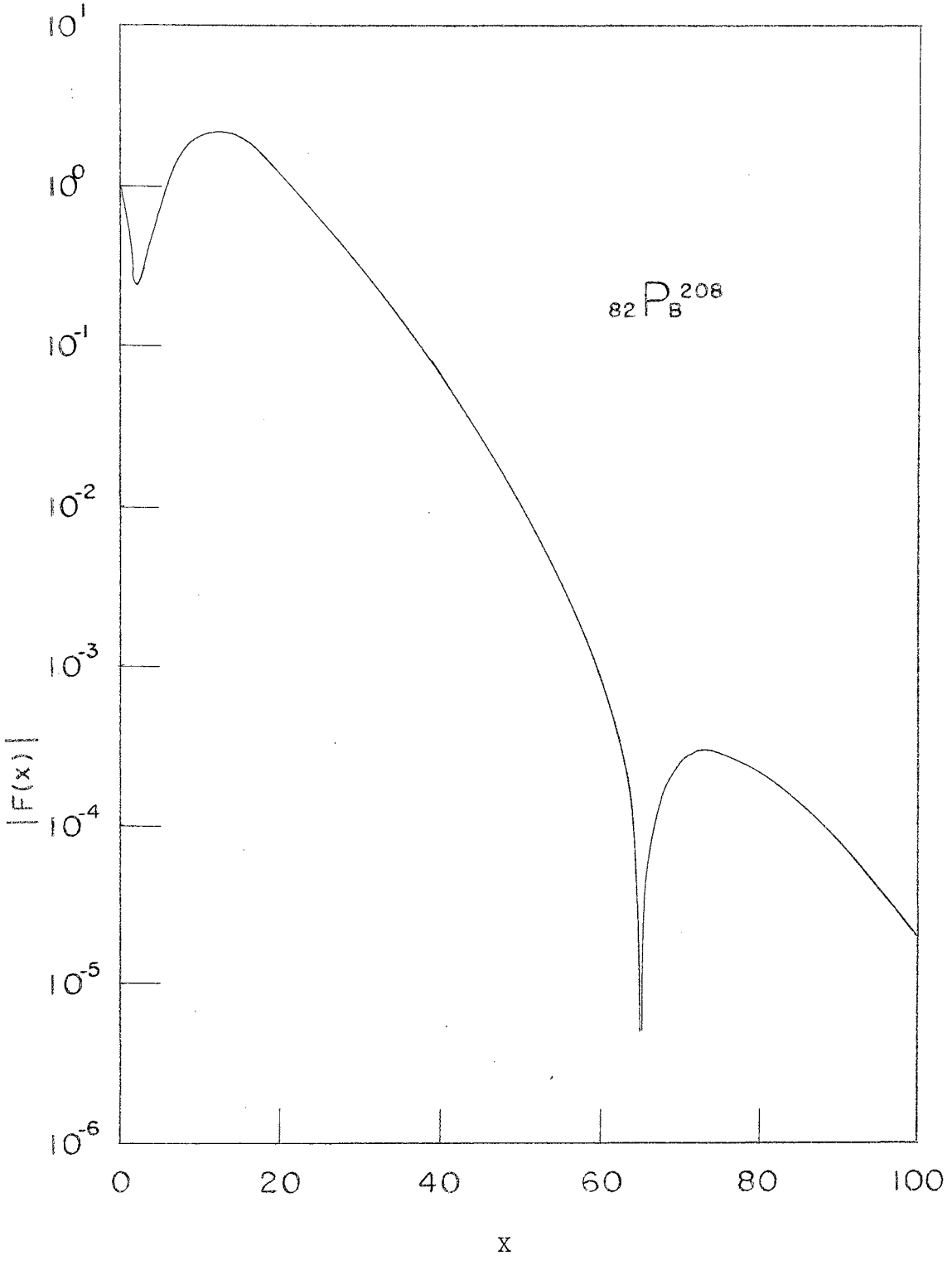

Figure 10. Absolute Value of the Form Factor for Pb^{208}

ample, has three zeros in the EHO model.) The EHO predicts from zero to five minima, however, with the number of minima increasing as z increases.

In Figures (6) through (10), we present a plot of $|F(q)|$ as a function of its arguement (q^2/α^2):

$$F(q) \longrightarrow F(x) = \sum_{m=0}^{m'} C_m x^m e^{-\frac{1}{4}x} \tag{80}$$

$$q^2/\alpha^2 \longrightarrow x \tag{81}$$

We are now in a position to discuss the cross-sections predicted by our model. By putting in the physical constants (z, e, M, etc.) and evaluating Equation (73) as a function of the scattering angle θ, we can compare the predicted cross-sections with the experimental data reported in the literature (25, 28, 41, 42, 45). To aid in evaluating these cross-sections, a computer program was written and is presented in Appendix E. In Figures (11) through (18), we show the differential cross-section $d\sigma/d\Omega$ as a function of the scattering angle θ (measured in the lab frame) for the five nuclei mentioned earlier (He^4, C^{12}, Ca^{40}, In^{115}, Pb^{208}).

In Figure 11, 800 MeV electrons are scattered by He^4 nuclei. As shown, we have presented cross-sections for both $\kappa = +1$ and $\kappa = -1$ configurations. The EHO predicts a diffraction minimum in each case, but for the $\kappa = +1$ configuration, the minimum occurs at a momentum transfer (scattering angle) that is greater than q for 80^o. As we can see, none of the three provides a very good fit to the data. Figure 12 shows what is generally known--that the harmonic oscillator provides an excellent model of the charge distribution in C^{12} (39). Figures 13, 14, and 15

investigate the effect an increase in the incident energy E_o has on the agreement. As shown, the fit does not seem to depend on the energy of the incident particles. Figure 16 shows that the agreement between the EHO and experiment improves somewhat as we go to heavier nuclei. Although the shape is not very accurate, the magnitude of the predicted cross-sections is rather close to the experimental points. Finally, Figures 17 and 18 show a fair agreement in the case of lead. Although each predicted curve is too small, the shape of the curves follows very closely the behavior of the experimental cross-sections. Again, as in the case of calcium, no significant change was observed for different incident energies.

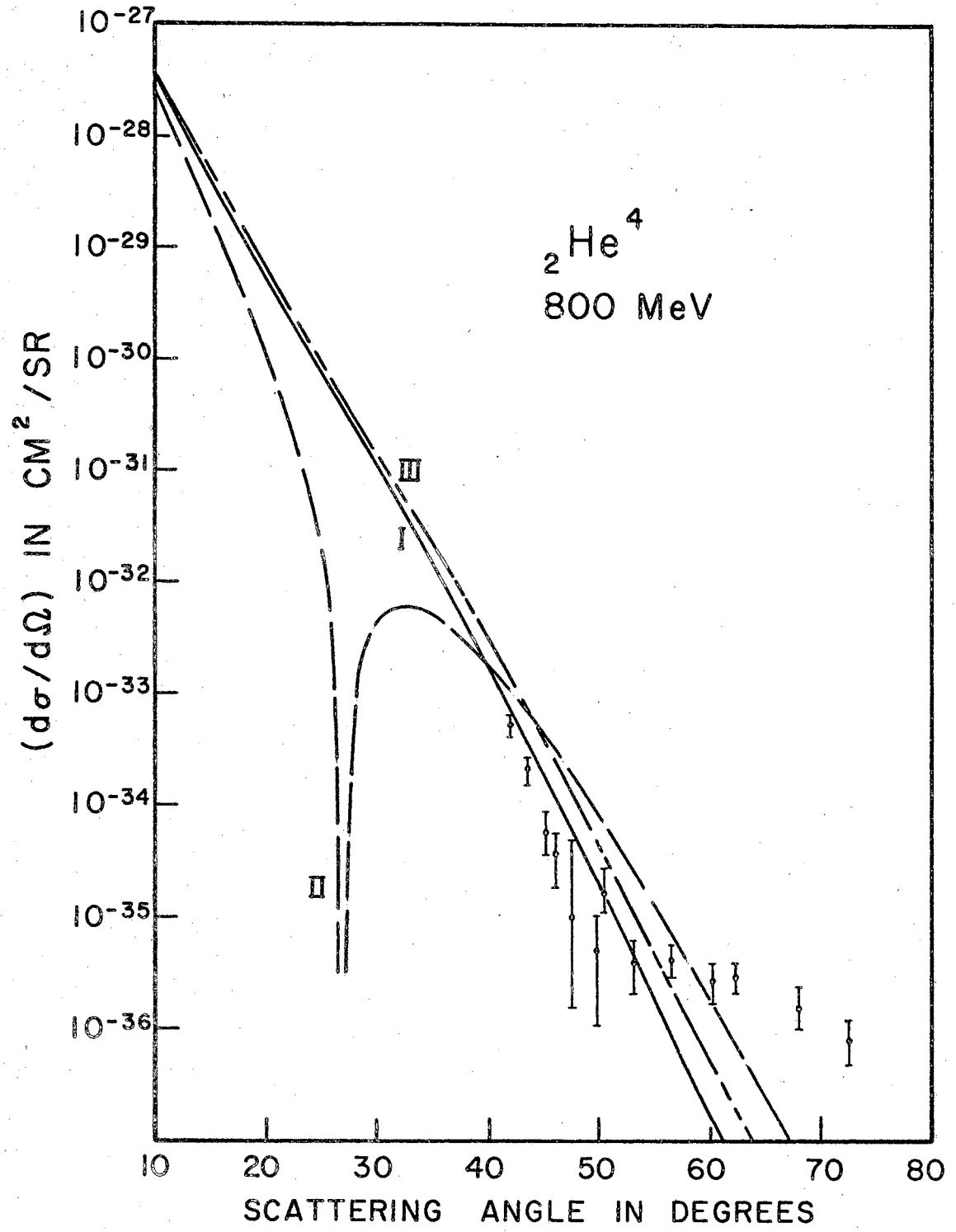

Figure 11. Differential Cross-Sections for Elastic Scattering of 800 MeV Electrons by Helium. Curve I is predicted by the NRHO. Curve II is predicted by the EHO with $\kappa = -1$, and curve III is predicted by the EHO with $\kappa = +1$. Experimental points from reference (41).

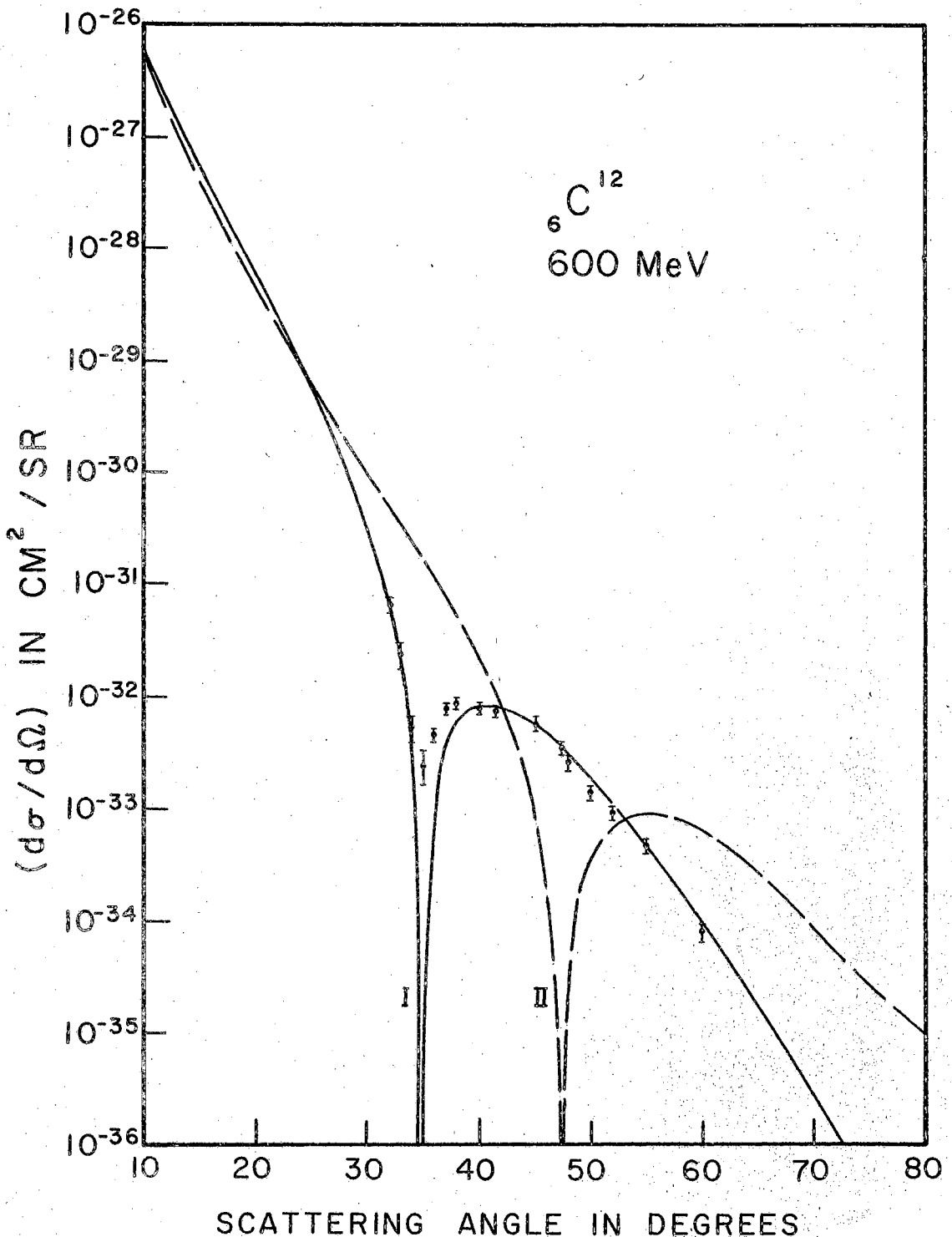

Figure 12. Differential Cross-Sections for Elastic Scattering of 600 MeV Electrons from Carbon. Curve I is predicted by the NRHO, and curve II is predicted by the EHO. Experimental points from reference (39).

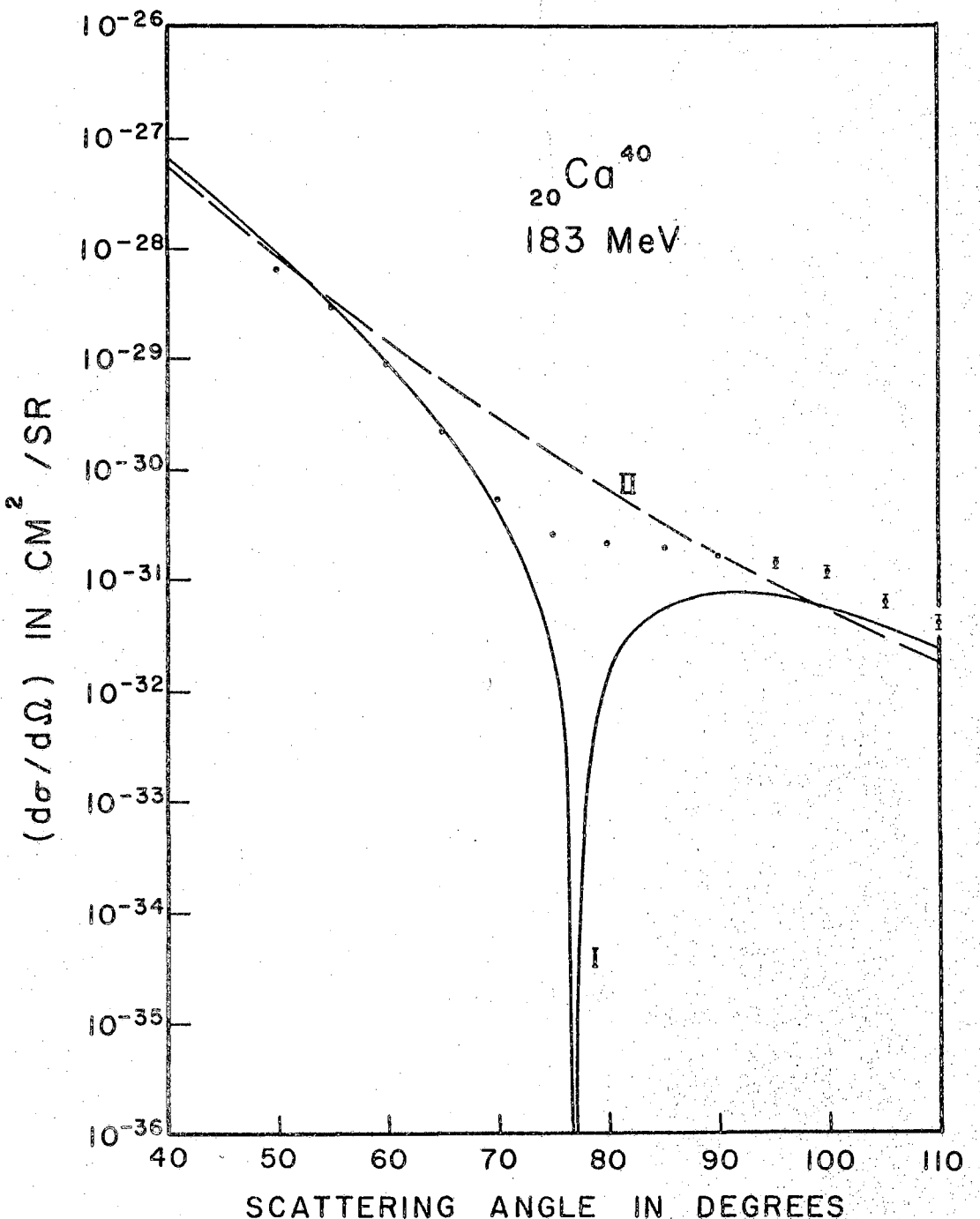

Figure 13. Differential Cross-Sections for Elastic Scattering of 183 MeV Electrons from Calcium. Curve I is predicted by the NRHO, and curve II is predicted by the EHO. Experimental points from reference (25).

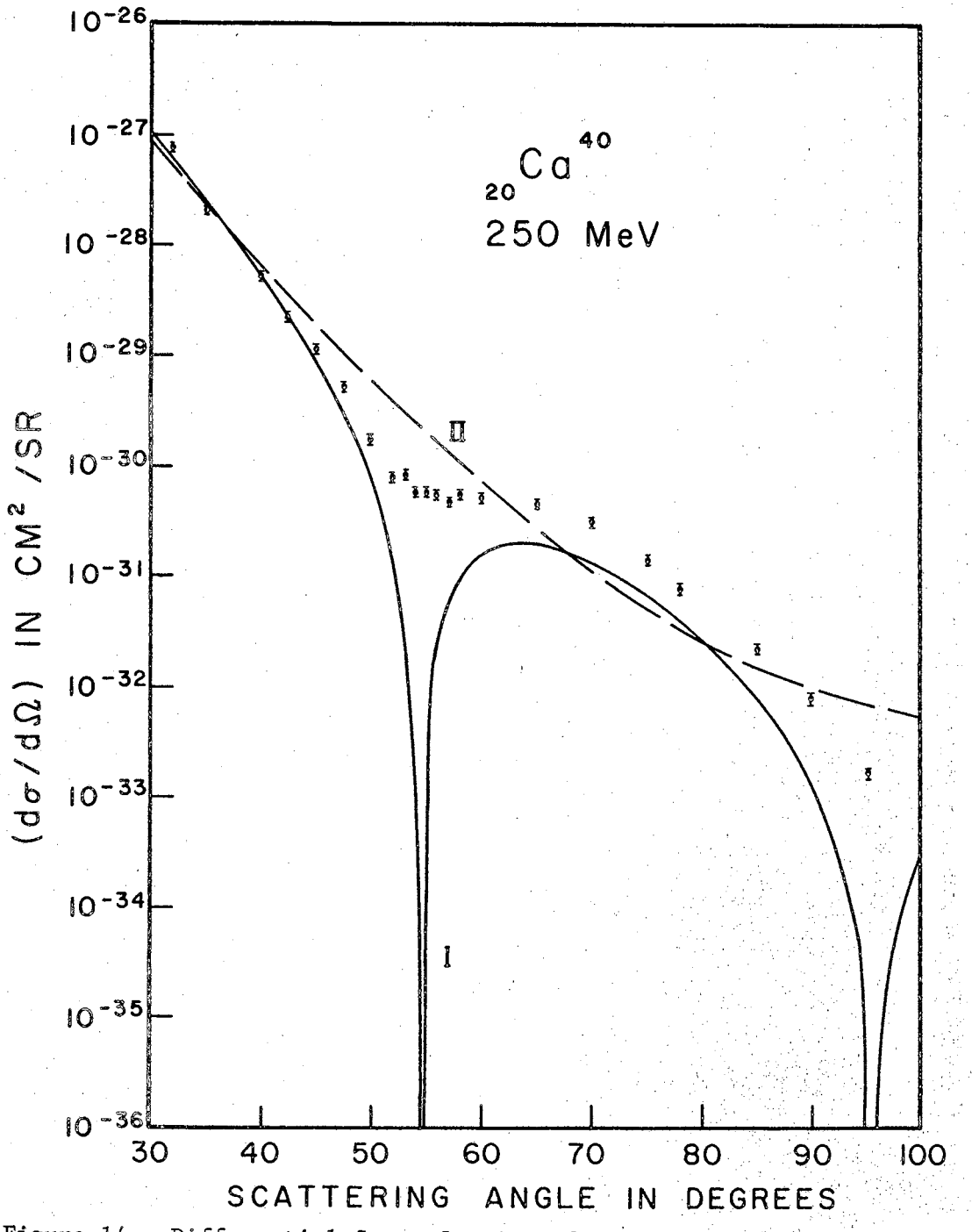

Figure 14. Differential Cross-Sections for Elastic Scattering of 250 MeV Electrons from Calcium. Curve I is predicted by the NRHO, and curve II is predicted by the EHO. Experimental points from reference (37).

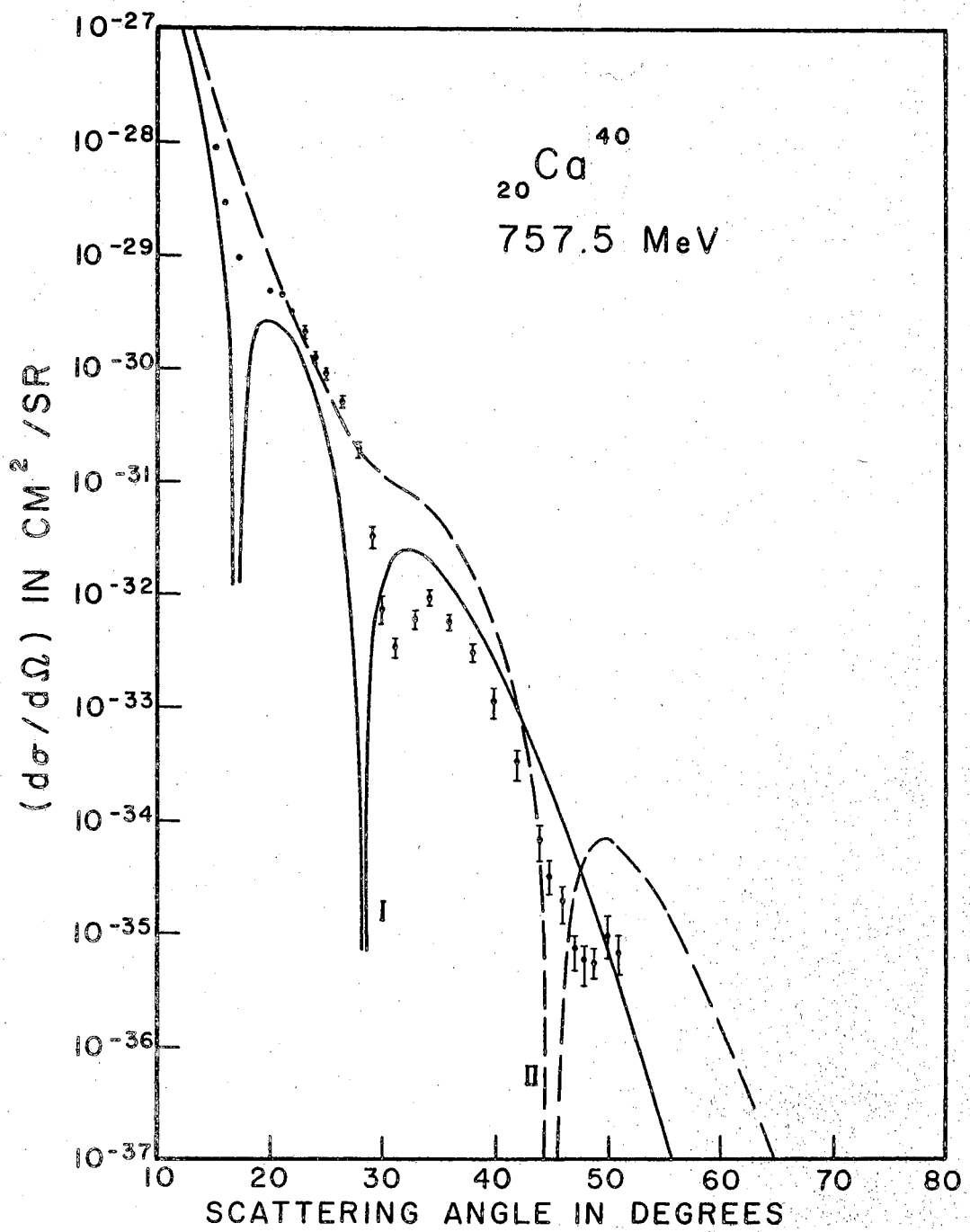

Figure 15. Differential Cross-Sections for Elastic Scattering of 757.5 MeV Electrons from Calcium. Curve I is predicted by the NRHO, and curve II is predicted by the EHO. Experimental points from reference (24).

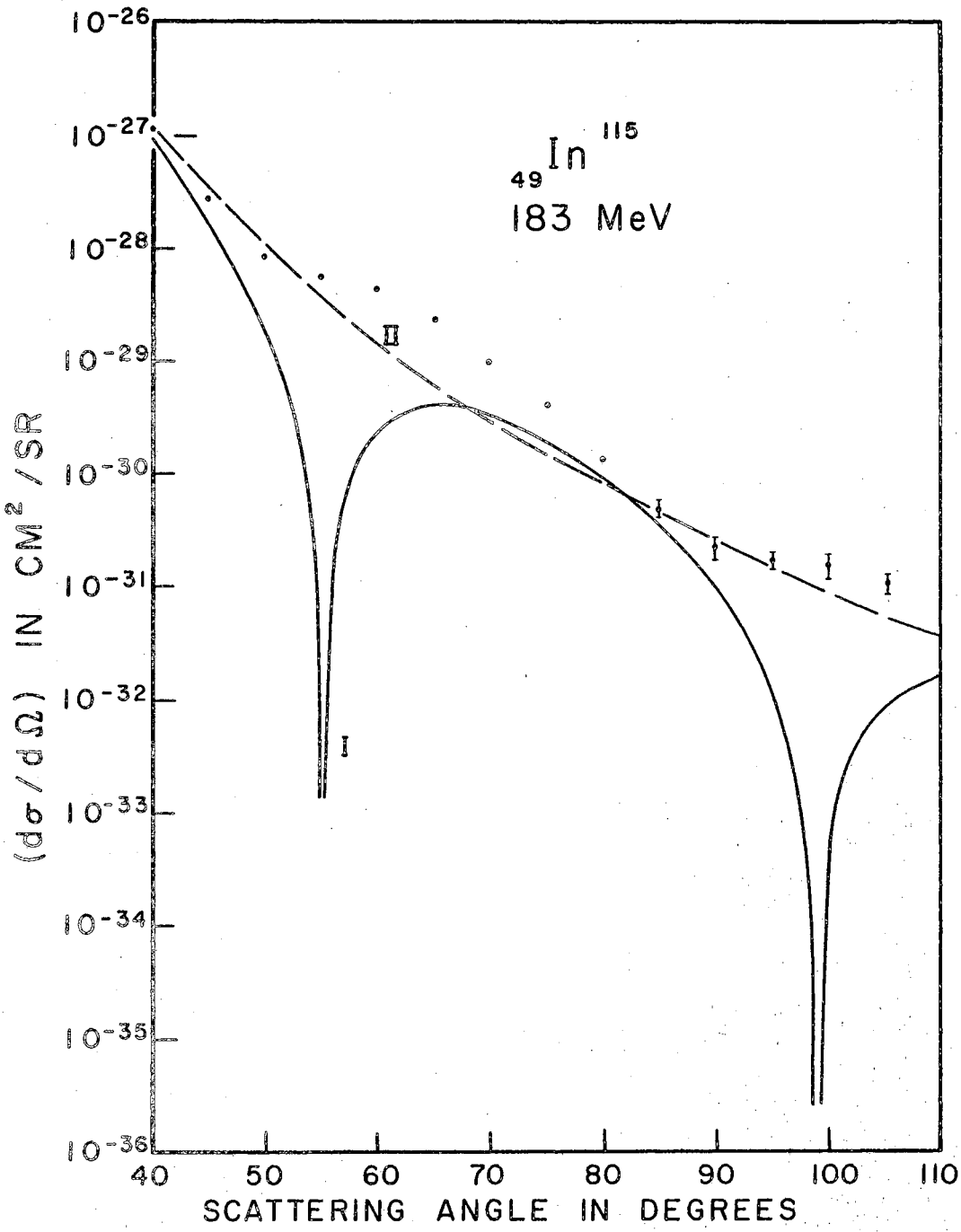

Figure 16. Differential Cross-Sections for Elastic Scattering of 183 MeV Electrons from Indium. Curve I is predicted by the NRHO, and curve II is predicted by the EHO. Experimental points from reference (25).

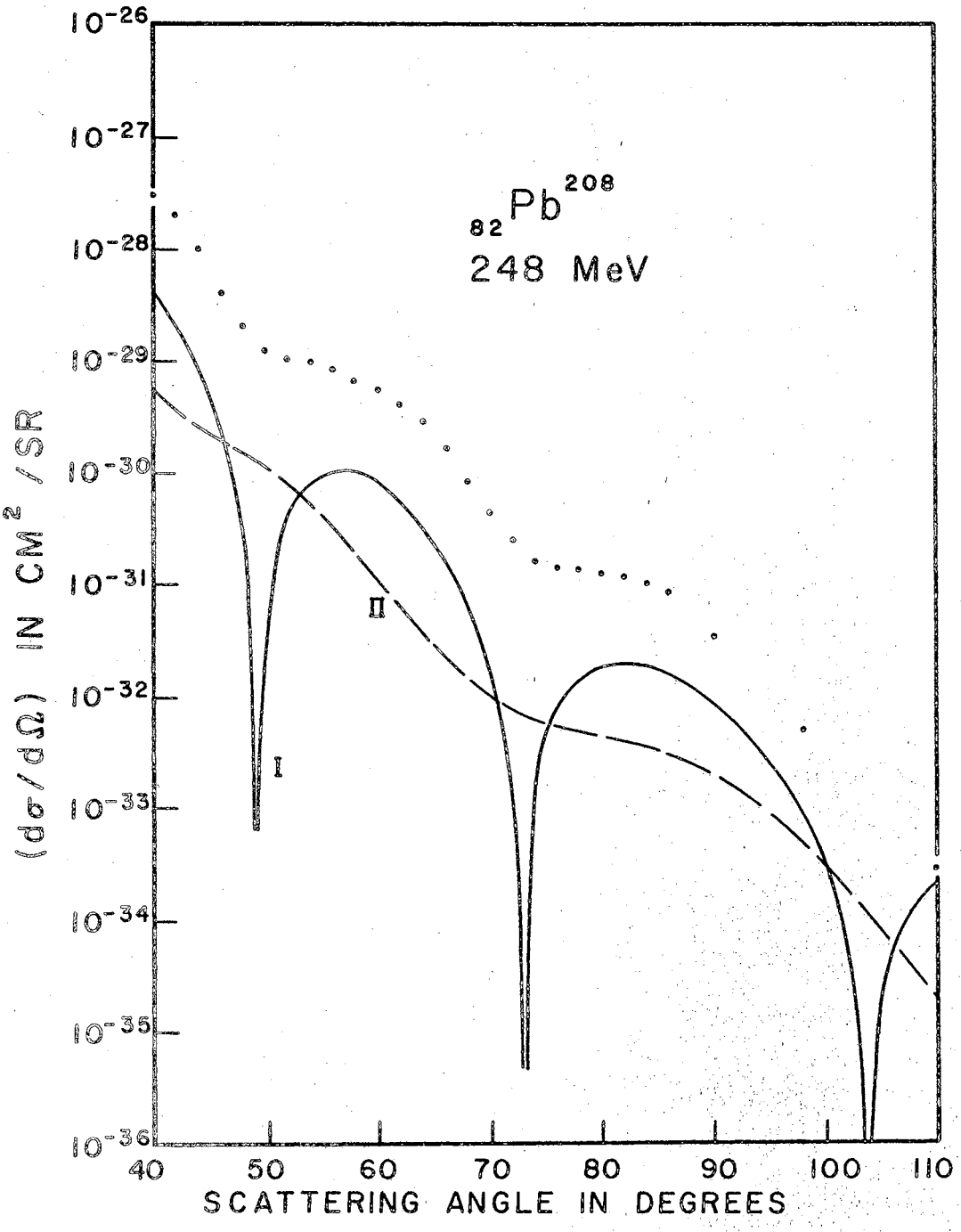

Figure 17. Differential Cross-Sections for Elastic Scattering of 248 MeV Electrons from Lead. Curve I is the NRHO model, and curve II is the EHO model. Experimental points from reference (45).

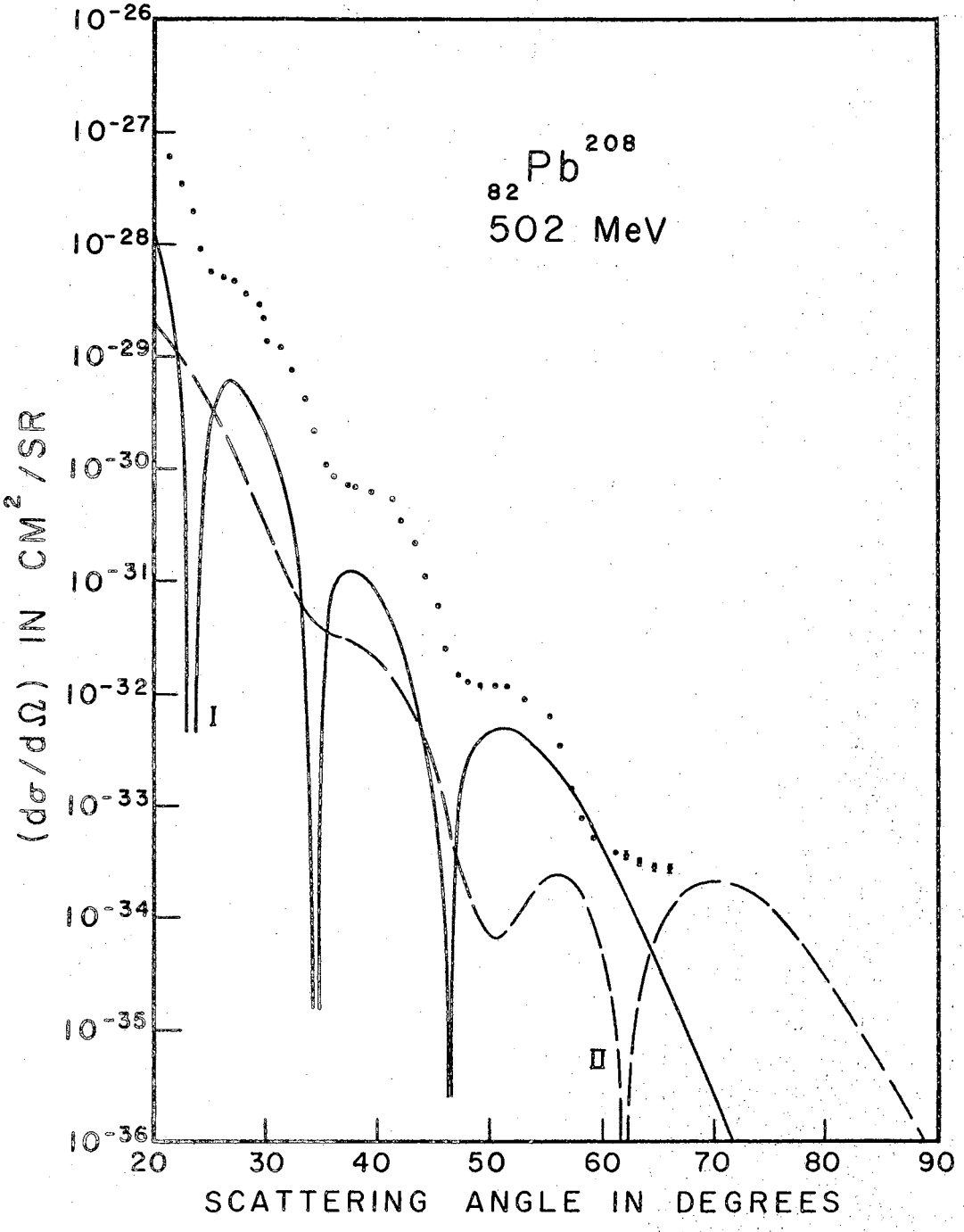

Figure 18. Differential Cross-Sections for Elastic Scattering of 502 MeV Electrons from Lead. Curve I is the NRHO model, and curve II is the EHO model. Experimental points from reference (45).

CHAPTER V

CONCLUSIONS

In view of the absence of a discussion of relativistic nuclear motions, and motivated by the availability of a single-particle Hamiltonian, we felt it worthwhile to investigate the regions of nuclei where relativistic effects could possibly be significant. The Dirac equation with a Coulomb potential can only describe the Coulomb effects in the nucleus, which are much weaker than the nuclear forces. On the other hand, the harmonic oscillator has long been in use as a single-particle nuclear model in non-relativistic descriptions. The EHO then happens to be a good example of a relativistic model. The most interesting case of the triton (10) has been investigated by more exact two-body methods, even taking into account relativistic interactions, but the case of intermediate and heavy nuclei cannot be treated as easily, except through an (approximate) single-particle model.

The energy spectrum of the EHO suggested the possibility of a relativistic shell structure and hence, this was investigated. However, the many level degeneracy, especially the independence of the energy on the sign of κ, introduced an arbitrariness in the level sequence. When, guided by the non-relativistic limit of the EHO, obtained through a Foldy-Wouthuysen transformation, the states are filled in accordance with the Mayer-Jensen (22) scheme, that is, assuming $j = \ell + \frac{1}{2}$ to be lower in energy than $j = \ell - \frac{1}{2}$, it turns out that the magic numbers

50, 82, 126 are not observed. In the other extreme, a purely arbitrary arrangement of κ substates happens to give all the magic numbers as well as the semimagic numbers 14 and 40. In any case, it is important to note that no splitting of κ substates is necessary to identify the magic numbers. What is of interest is the essential point that shall structure can be obtained, even with relativistic nuclear motions, and this fact is brought out in Table (II).

Since this is a one body model, and since simple, analytical wave functions are available, it is important to ask how well the experimental electron-nucleus scattering experiments of Hofstadter and his co-workers agree with the predictions of this model. It is well known that these high-energy elastic scattering experiments are about the best possible evidence of nuclear structure, since the deBroglie wavelength of these electrons becomes comparable to the linear extension of the nucleus and the electrons can then probe the interior of the nucleus. The analysis of these experiments is done most easily in the first Born approximation, where the nuclear structure effects appear in the form factor, which is essentially the Fourier transform with respect to the momentum transfer of the charge distribution in the nucleus. The normalized wave functions of the EHO help in expressing the charge density in closed form, and this leads to a simple expression for the form factor. One of the merits of the harmonic oscillator potential happens to be the fact that only one arbitrary parameter exists--the oscillator constant, α. Since the size of the nucleus depends on α, we can evaluate the oscillator constant by a comparison of the nuclear densities.

This numerical parameter (α) has been used to calculate the cross-sections for five nuclei: He^4, C^{12}, Ca^{40}, In^{115}, and Pb^{208}. From the

viewpoint of wave mechanics, the potential sphere of the nucleus diffracts the short wavelengths of the (high energy) electron waves, and thus the location and number of diffraction minima are a matter of interest. In our analysis, these can be obtained from the polynomial multiplying the Gaussian exponential in the form factor. The momentum transfer ($\hbar q$) is a good kinematical variable, and the scattering cross-sections are functions of this variable. The results of this comparison are shown in Figures (11) - (18), together with the predictions of the NRHO. Our choice of these five nuclei was made to provide a representative collection from different values of Z and with the requirement that experimental data be available for comparison.

There are two essential points that emerge from our investigation. In almost every case, the EHO shows a much greater central density, indicating that a tighter binding energy and larger kinetic energy is indicated. The EHO shows a pronounced central peak, followed by a rapid fall-off at the surface, implying that relativistic effects prevent a clustering of the protons at the surface and draw them in toward the center. As far as the actual cross-sections are concerned, the relativistic fits are unsatisfactory, except perhaps for heavy nuclei such as lead. Lead is known to be a very tightly packed nucleus, resulting in relatively high kinetic energies, so it is not surprising that the EHO is most appropriate for large, dense, nuclei. The result of our study has been to show that, except for exceptional cases (extremely light and extremely heavy nuclei) the nuclear motions do not seem to be relativistic, and an estimate of the average nucleon velocity on the basis of the EHO shows that the speeds of the nucleons rarely exceeds 20% of the speed of light.

Ever since the discovery of rotational energy levels, it has been an accepted opinion that the nuclei are deformed, and the Nilsson model is considered to be an adequate description. We have shown that Hamiltonian possessing exact eigenvectors can be simply constructed from the EHO Hamiltonian, and the terms in its non-relativistic limit can be put into a one-to-one correspondence with the terms in the Nilsson Hamiltonian. We can interpret this to mean that a contributory cause for deformations may be of relativistic origin--say the relativistic variation of mass with velocity of the particles in unfilled shells may contribute to polarization of the core.

As is well known, the most realistic nuclear model has to be based on the many-body approach. (See reference 59). From what we have seen, it does not seem that the basic two-particle interaction is described very closely by the EHO Hamiltonian.

REFERENCES

1. Blochinzew, D. Physik. Zeits. Sowjetunion 8, 270 (1935).

2. Margenau, H. Phys. Rev. 50, 342 (1936).

3. Feenberg, E. Phys. Rev. 50, 674 (1936).

4. Share, S. and G. Breit. Phys. Rev. 52, 546 (1937).

5. Primakoff, H. Phys. Rev. 72, 118 (1947).

6. Breit, G. Phys. Rev. 51, 248 (1937).

7. Breit, G. Phys. Rev. 53, 153 (1937).

8. Siegel, A. Phys. Rev. 82, 194 (1950).

9. Breit, G. Phys. Rev. 71, 400 (1947).

10. Blatt, J. and V. Weisskopf. Theoretical Nuclear Physics. John Wiley and Sons, Inc., New York, 1952. p. 199.

11. Swamy, N. V. V. J. Phys. Rev. 180, 1225 (1969).

12. Flugge, S. and H. Marschall. Rechenmethoden der Quantentheorie, Erster Teil. Springer-Verlag, Berlin, 1952. p. 101.

13. Condon, E. and G. Shortley. The Theory of Atomic Spectra. Cambridge Univ. Press, Cambridge, 1951. Chapter III.

14. Erdelyi, A. et al. Higher Transcendental Functions. McGraw-Hill, Inc., New York, 1953. Vol. I, Chapter 6.

15. Melvin, M. and N. V. V. J. Swamy. J. Math Phys. 36, 157 (1957).

16. Rose, M. E. Relativistic Electron Theory. J. Wiley and Sons, Inc., New York, 1961.

17. Wigner, E. Group Theory and its Application to the Quantum Mechanics of Atomic Spectra. Academic Press, Inc., New Yor, 1959.

18. Biedenharn, L. C. and M. E. Rose. Rev. Mod. Phys. 25, 729 (1953).

19. Foldy, L. and S. Wouthuysen. Phys. Rev. 78, 29 (1950).

20. Lee, T. D. and C. N. Yang. Phys. Rev. 105, 1671 (1957).

21. Nilsson, S. Kgl. Danske Videnskab. Selskab, Mat.-Fys. Medd. 29, No. 16 (1955).

22. Mayer, M. and J. Jensen. Elementary Theory of Nuclear Shell Structure.

23. Erdelyi, A. Tables of Integral Transforms. McGraw-Hill Co., New York, 1954. Vol. I.

24. Bellicard, J. et al. Phys. Rev. Letters 19, 527 (1967).

25. Hofstadter, R. Rev. Mod. Phys. 28, 214 (1956).

26. Hofstadter, R. Ann. Rev. Nuc. Sci. 7, 231 (1957).

27. Ravenhall, D. Rev. Mod. Phys. 30, 430 (1958).

28. Ehrenberg, et al. Phys. Rev. 113, 666 (1959).

29. Meyer-Berkhout, U. et al. Annals of Physics 8, 119 (1959).

30. Burleson, G. and H. Kendall. Nuc. Phys. 19, 68 (1960).

31. Crannell, H. et al. Phys. Rev. 121, 283 (1961).

32. Crannell, H. and T. Griffy. Phys. Rev. 136, B1580 (1964).

33. Goldemberg, J. Phys. Lett. 16, 141 (1965).

34. Repellin, J. et al. Phys. Lett. 16, 169 (1965).

35. Frosch, R. et al. Phys. Lett. 21, 598 (1966).

36. Frank, H. et al. Phys. Lett. 19, 391 (1965).

37. Croissaux, M. et al. Phys. Rev. 137, B865 (1965).

38. Van Oostrum, K. Phys. Rev. Letters 16, 528 (1966).

39. Crannell, H. Phys. Rev. 148, 1107 (1966).

40. Bellicard, J. and K. Van Oostrum. Phys. Rev. Lett. 19, 242 (1967).

41. Frosch, R. et al. Phys. Rev. 160, 874 (1967).

42. Frosch, R. et al. Phys. Rev. 174, 1380 (1968).

43. Donnelly, T. W. and G. E. Walker. Phys. Rev. Letters 22, 1121 (1969).

44. Dally, E. et al. Phys. Rev. (to be published).

45. Heisenberg, J. Phys. Rev. Letters 23, 1402 (1969).

46. Van Niftrik, G. Nuclear Physics A131, 574 (1969).

47. Singhal, R. et al. Phys. Rev. Letters 24, 73 (1970).

48. Hofstadter, R. Nuclear and Nucleon Structure. W. A. Benjamin, Inc., New York, 1963.

49. Elton, L. R. B. Nuclear Sizes. Oxford Univ. Press, London, 1961.

50. Rose, M. E. Phys. Rev. 73, 279 (1948).

51. Schweber, S. and H. Bethe and F. de Hoffmann. Mesons and Fields. Row, Peterson, and Co., Evanston, 1956. Vol. I.

52. Schiff, L. I. Phys. Rev. 92, 988 (1953).

53. Schiff, L. I. Phys. Rev. 96, 765 (1954).

54. Smith, J. H. Phys. Rev. 95, 271 (1954).

55. Mott, N. F. Proc. Roy. Soc. (London) A124, 426 (1929).

56. Mott, N. F. Proc. Roy. Soc. (London) A135, 429 (1932).

57. Abramowitz, M. and I. Stegun, ed. Handbook of Mathematical Functions. Dover Publications, Inc., New York, 1965.

58. Mishina, A. and I. Proskuryakov. Higher Algebra. Pergamon Press, Oxford, 1965. p. 196.

59. Brueckner, K., A. Lockett and M. Rotenberg. Phys. Rev. 121, 255 (1961).

60. "System/360 Scientific Subroutine Package (360A-CM-03X) Version III Programmer's Manual". International Business Machines Corp., White Plains, N.Y., 1968.

APPENDIX A

The normalized radial eigenfunctions of the NRHO are given by the expression

$$F_{v\ell}(r) = \sqrt{\frac{2\alpha^3\,\Gamma(v+\ell+3/2)}{v!\,[\Gamma(\ell+\frac{3}{2})]^2}}\,(\alpha r)^{\ell}\, e^{-\frac{1}{2}(\alpha r)^2}\, {}_1F_1\left(-v, \ell+\tfrac{3}{2};\ \alpha^2 r^2\right)$$

We list here the explicit values of $F_{v\ell}$ for v = 0, 1, 2 and ℓ = 0, 1, 2, 3, 4.

$$F_{00} = \sqrt{\frac{4\alpha^3}{\pi^{1/2}}}\; e^{-\frac{1}{2}\alpha^2 r^2}$$

$$F_{01} = \sqrt{\frac{8}{3}\,\frac{\alpha^3}{\pi^{1/2}}}\; e^{-\frac{1}{2}\alpha^2 r^2}$$

$$F_{02} = \sqrt{\frac{16}{15}\,\frac{\alpha^3}{\pi^{1/2}}}\; e^{-\frac{1}{2}\alpha^2 r^2}$$

$$F_{03} = \sqrt{\frac{32}{105}\,\frac{\alpha^3}{\pi^{1/2}}}\; e^{-\frac{1}{2}\alpha^2 r^2}$$

$$F_{04} = \sqrt{\frac{64}{945}\,\frac{\alpha^3}{\pi^{1/2}}}\; e^{-\frac{1}{2}(\alpha^2 r^2)}$$

. . . . . .

$$F_{10} = \sqrt{\frac{8}{3}\frac{\alpha^3}{\pi^{1/2}}}\left[\frac{3}{2} - (\alpha r)^2\right] e^{-\frac{1}{2}\alpha^2 r^2}$$

$$F_{11} = \sqrt{\frac{16}{15}\frac{\alpha^3}{\pi^{1/2}}}\left[\frac{5}{2}(\alpha r) - (\alpha r)^3\right] e^{-\frac{1}{2}\alpha^2 r^2}$$

$$F_{12} = \sqrt{\frac{32}{105}\frac{\alpha^3}{\pi^{1/2}}}\left[\frac{7}{2}(\alpha r)^2 - (\alpha r)^4\right] e^{-\frac{1}{2}\alpha^2 r^2}$$

$$F_{13} = \sqrt{\frac{64}{945}\frac{\alpha^3}{\pi^{1/2}}}\left[\frac{9}{2}(\alpha r)^3 - (\alpha r)^5\right] e^{-\frac{1}{2}\alpha^2 r^2}$$

$$F_{14} = \sqrt{\frac{128}{10395}\frac{\alpha^3}{\pi^{1/2}}}\left[\frac{11}{2}(\alpha r)^4 - (\alpha r)^6\right] e^{-\frac{1}{2}\alpha^2 r^2}$$

.....

$$F_{20} = \sqrt{\frac{16}{15}\frac{\alpha^3}{\pi^{1/2}}}\left[\frac{15}{4} - 5(\alpha r)^2 + (\alpha r)^4\right] e^{-\frac{1}{2}\alpha^2 r^2}$$

$$F_{21} = \sqrt{\frac{32}{105}\frac{\alpha^3}{\pi^{1/2}}}\left[\frac{35}{4}(\alpha r) - 7(\alpha r)^3 + (\alpha r)^5\right] e^{-\frac{1}{2}\alpha^2 r^2}$$

$$F_{22} = \sqrt{\frac{64}{945}\frac{\alpha^3}{\pi^{1/2}}}\left[\frac{63}{4}(\alpha r)^2 - 9(\alpha r)^4 + (\alpha r)^6\right] e^{-\frac{1}{2}\alpha^2 r^2}$$

$$F_{23} = \sqrt{\frac{128}{10395}\frac{\alpha^3}{\pi^{1/2}}}\left[\frac{99}{4}(\alpha r)^3 - 11(\alpha r)^5 + (\alpha r)^7\right] e^{-\frac{1}{2}\alpha^2 r^2}$$

$$F_{24} = \sqrt{\frac{256}{135135}\frac{\alpha^3}{\pi^{1/2}}}\left[\frac{143}{4}(\alpha r)^4 - 13(\alpha r)^6 + (\alpha r)^8\right] e^{-\frac{1}{2}\alpha^2 r^2}$$

- - - - - - - - - - -

APPENDIX B

The Pauli spinors

$$\chi_{\kappa}^{\mu} = \begin{pmatrix} C^{\ell\ \frac{1}{2}\ j}_{\mu-\frac{1}{2}\ \frac{1}{2}\ \mu}\, Y_{\ell}^{\mu-\frac{1}{2}} \\ C^{\ell\ \frac{1}{2}\ j}_{\mu+\frac{1}{2}\ -\frac{1}{2}\ \mu}\, Y_{\ell}^{\mu+\frac{1}{2}} \end{pmatrix}$$

and

$$\chi_{-\kappa}^{\mu} = \begin{pmatrix} C^{\bar{\ell}\ \frac{1}{2}\ j}_{\mu-\frac{1}{2}\ \frac{1}{2}\ \mu}\, Y_{\bar{\ell}}^{\mu-\frac{1}{2}} \\ C^{\bar{\ell}\ \frac{1}{2}\ j}_{\mu+\frac{1}{2}\ -\frac{1}{2}\ \mu}\, Y_{\bar{\ell}}^{\mu+\frac{1}{2}} \end{pmatrix}$$

form the spin-angle part of the EHO wave functions. Below, we list values of χ_{κ}^{μ} and $\chi_{-\kappa}^{\mu}$ for $|\kappa| = 1, 2, 3, 4$. For each value of κ, μ can take on $2|\kappa|$ values.

$$\kappa = +1: \quad \chi_{\kappa}^{\mu} = \begin{pmatrix} -\sqrt{\frac{\frac{3}{2}-\mu}{3}}\, Y_{1}^{\mu-\frac{1}{2}} \\ \sqrt{\frac{\frac{3}{2}+\mu}{3}}\, Y_{1}^{\mu+\frac{1}{2}} \end{pmatrix} \quad ; \quad \chi_{-\kappa}^{\mu} = \begin{pmatrix} -\sqrt{\frac{\frac{1}{2}-\mu}{1}}\, Y_{0}^{\mu-\frac{1}{2}} \\ \sqrt{\frac{\frac{1}{2}+\mu}{1}}\, Y_{0}^{\mu+\frac{1}{2}} \end{pmatrix}$$

$$\kappa = -1: \quad \chi_{\kappa}^{\mu} = \begin{pmatrix} \sqrt{\frac{\mu+\frac{1}{2}}{1}}\, Y_{0}^{\mu-\frac{1}{2}} \\ \sqrt{\frac{-\mu+\frac{1}{2}}{1}}\, Y_{0}^{\mu+\frac{1}{2}} \end{pmatrix} \quad ; \quad \chi_{-\kappa}^{\mu} = \begin{pmatrix} \sqrt{\frac{\mu+3/2}{3}}\, Y_{1}^{\mu-\frac{1}{2}} \\ \sqrt{\frac{-\mu+3/2}{3}}\, Y_{1}^{\mu+\frac{1}{2}} \end{pmatrix}$$

$$\kappa=+2: \quad \chi^{\mu}_{\kappa} = \begin{pmatrix} -\sqrt{\frac{-\mu+5/2}{5}}\, Y_2^{\mu-\frac{1}{2}} \\ \sqrt{\frac{\mu+5/2}{5}}\, Y_2^{\mu+\frac{1}{2}} \end{pmatrix}; \quad \chi^{\mu}_{-\kappa} = \begin{pmatrix} -\sqrt{\frac{-\mu+3/2}{3}}\, Y_1^{\mu-\frac{1}{2}} \\ \sqrt{\frac{\mu+3/2}{3}}\, Y_1^{\mu+\frac{1}{2}} \end{pmatrix}$$

$$\kappa=-2: \quad \chi^{\mu}_{\kappa} = \begin{pmatrix} \sqrt{\frac{\mu+\frac{3}{2}}{3}}\, Y_1^{\mu-\frac{1}{2}} \\ \sqrt{\frac{-\mu+\frac{3}{2}}{3}}\, Y_1^{\mu+\frac{1}{2}} \end{pmatrix}; \quad \chi^{\mu}_{-\kappa} = \begin{pmatrix} \sqrt{\frac{\mu+5/2}{5}}\, Y_2^{\mu-\frac{1}{2}} \\ \sqrt{\frac{-\mu+5/2}{5}}\, Y_2^{\mu+\frac{1}{2}} \end{pmatrix}$$

$$\kappa=+3: \quad \chi^{\mu}_{\kappa} = \begin{pmatrix} -\sqrt{\frac{-\mu+7/2}{7}}\, Y_3^{\mu-\frac{1}{2}} \\ \sqrt{\frac{\mu+7/2}{7}}\, Y_3^{\mu+1/2} \end{pmatrix}; \quad \chi^{\mu}_{-\kappa} = \begin{pmatrix} -\sqrt{\frac{-\mu+5/2}{5}}\, Y_2^{\mu-\frac{1}{2}} \\ \sqrt{\frac{\mu+5/2}{5}}\, Y_2^{\mu+1/2} \end{pmatrix}$$

$$\kappa=-3: \quad \chi^{\mu}_{\kappa} = \begin{pmatrix} \sqrt{\frac{\mu+\frac{5}{2}}{5}}\, Y_2^{\mu-\frac{1}{2}} \\ \sqrt{\frac{-\mu+\frac{5}{2}}{5}}\, Y_2^{\mu+\frac{1}{2}} \end{pmatrix}; \quad \chi^{\mu}_{-\kappa} = \begin{pmatrix} \sqrt{\frac{\mu+7/2}{7}}\, Y_3^{\mu-\frac{1}{2}} \\ \sqrt{\frac{-\mu+7/2}{7}}\, Y_3^{\mu+\frac{1}{2}} \end{pmatrix}$$

$$\kappa=+4: \quad \chi^{\mu}_{\kappa} = \begin{pmatrix} -\sqrt{\frac{\mu+9/2}{9}}\, Y_4^{\mu-\frac{1}{2}} \\ \sqrt{\frac{-\mu+9/2}{9}}\, Y_4^{\mu+\frac{1}{2}} \end{pmatrix}; \quad \chi^{\mu}_{-\kappa} = \begin{pmatrix} -\sqrt{\frac{-\mu+7/2}{7}}\, Y_3^{\mu-\frac{1}{2}} \\ \sqrt{\frac{\mu+7/2}{7}}\, Y_3^{\mu+1/2} \end{pmatrix}$$

$$\kappa=-4: \quad \chi^{\mu}_{\kappa} = \begin{pmatrix} -\sqrt{\frac{\mu+7/2}{7}}\, Y_3^{\mu-\frac{1}{2}} \\ \sqrt{\frac{-\mu+7/2}{7}}\, Y_3^{\mu+1/2} \end{pmatrix}; \quad \chi^{\mu}_{-\kappa} = \begin{pmatrix} -\sqrt{\frac{-\mu+9/2}{7}}\, Y_4^{\mu-\frac{1}{2}} \\ \sqrt{\frac{\mu+9/2}{7}}\, Y_4^{\mu+\frac{1}{2}} \end{pmatrix}$$

APPENDIX C

This program, written in the Fortran IV language, will print out the coefficients of the NRHO and EHO radial densities for the single-particle states up through $(v,\ell) = (5,5)$. It then adds the first z of these states together, giving the coefficients of the nuclear density for as many nuclei are needed. (In its present form, the densities are given for z = 2, 6, 20, 52, 49, 82.) Having done this, the program evaluates the normalization integral

$$\text{CHECK} = 4\pi \int_0^\infty \rho(r)\ r^2\ dr$$

and prints this value for each nuclear density. (Our densities were to be normalized to unity.) Making use of equation (78), the coefficients in the form factor F(q) are then calculated and printed similarly. Execution time of this program for the six nuclei and 36 single-particle states is less than 30 seconds on the IBM 360/50.

```
     00000000011111111112222222222333333333344444444455555555566666666677777777778
     12345678901234567890123456789012345678901234567890123456789012345678901234567890
CARD
0001  $JOB
0002  C      THIS PROGRAM EVALUATES THE COEFFICIENTS O(I,KZ,K) IN THE RADIAL DENSITIES
0003         DIMENSION ITER(10),C(25),X(6,6,60),D(2,8,2),F(2,8,12)
0004         DOUBLE PRECISION X, D
0005      10 FORMAT (1H1,5X, 'RADIAL DENSITY: RHO (V,L)')
0006      20 FORMAT (1HO,5X,'RHO(',I1,',',I1,')= EXP(-A*A*R*R) *')
0007      30 FORMAT (1HO,20X,F17.14,' A**',I2,' R**',I2)
0008      40 FORMAT (6I4)
0009      50 FORMAT (1H1,10X, 'NON-RELATIVISTIC RADIAL DENSITIES RHO(Z)')
0010      60 FORMAT (1HO,5X,'Z=',I2,5X,'RHO= EXP(-A*A*R*R) *')
0011      70 FORMAT (1H1,10X,'RELATIVISTIC RADIAL DENSITIES RHO(Z)')
0012         READ (5,40) (ITER(JK),JK=1,6)
0013  C  THIS PART OF THE PROGRAM EVALUATES THE COEFFICIENTS IN THE SINGLE-PARTICLE
0014  C   DENSITIES OF THE IHO MODEL, X(N,KL,IEXA). HERE, N IS THE PRINCIPAL QUANTUM
0015  C   NUMBER (N=1,2,...), KL IS THE ORB. ANG. MOM. + 1, IEXA=POWER OF ALPHA.
0016         WRITE (6,10)
0017         J=0
0018         DO 12 N=1,6
0019         KV=N-1
0020         KT=2*KV+1
0021         DO 12 KL=1,6
0022         L=KL-1
0023         J=J+1
0024         WRITE (6,20) KV, L
0025         DO 1 LAMBDA =1,10
0026         XB=LAMBDA
0027         XL=L
0028         V=KV
0029         C(1)=1.0
0030      1  C(LAMBDA+1)=((XB-V-1.0)/((XB+XL+0.5)*XB))*C(LAMBDA)
0031  C      F1=GAMMA(V+L+3/2)
0032         F1=V+XL+0.5
0033         Y=F1
0034      2  Y=Y-1.0
0035         IF (Y.LT.0.5) GO TO 3
0036         F1=F1*Y
0037         GO TO 2
0038      3  F1=1.77245385*F1
0039  C      F2=GAMMA(V+1)
0040         F2=V
0041         IF (V.GE.2.0) GO TO 4
0042         F2=1.0
0043         GO TO 6
0044      4  Y=V
0045      5  Y=Y-1.0
0046         F2=F2*Y
0047         IF (Y.LE. 2.0) GO TO 6
0048         GO TO5
0049      6  CONTINUE
0050  C      F3=GAMMA(L+3/2)
0051         F3=XL+0.5
0052         Y=F3
0053      7  Y=Y-1.0
0054         IF (Y.LT. 0.5) GO TO 8
0055         F3=F3*Y
```

```
     00000000011111111112222222223333333334444444445555555556666666667777777778
     12345678901234567890123456789012345678901234567890123456789012345678901234567890
CARD
0056         GO TO 7
0057       8 F3=1.77245385*F3
0058         DO 11 MU=1,10
0059         SUM=0.0
0060         DO 9 LAMBDA=1,MU
0061         LDA=MU-LAMBDA+1
0062         TERM=C(LAMBDA)*C(LDA)
0063       9 SUM=SUM+TERM
0064         IEXA=2*MU+2*L+1
0065         IEXR=IEXA-3
0066         X(N,KL,IEXA)=SUM*F1/(6.2831853*F2*F3**2)
0067      11 WRITE(6,30) X(N,KL,IEXA),IEXA,IEXR
0068         X(N,2,3)=0.0
0069         X(N,3,3)=0.0
0070         X(N,3,5)=0.0
0071         X(N,4,3)=0.0
0072         X(N,4,5)=0.0
0073         X(N,4,7)=0.0
0074         X(N,5,3)=0.0
0075         X(N,5,5)=0.0
0076         X(N,5,7)=0.0
0077         X(N,5,9)=0.0
0078         X(N,6,3)=0.0
0079         X(N,6,5)=0.0
0080         X(N,6,7)=0.0
0081         X(N,6,9)=0.0
0082         X(N,6,11)=0.0
0083      12 CONTINUE
0084  C    THIS PART OF THE PROGRAM SUMS UP THE APPROPRIATE COEFFICIENTS IN THE  Z
0085  C    SINGLE PROTON STATES TO GIVE THE VECTOR OF COEFFICIENTS FOR THE TOTAL
0086  C    NUCLEAR DENSITY D(I, JK, K), WHERE: I=1-IHO MODEL, I=2-REL MODEL; JK LABELS
0087  C    THE NUCLEUS; K IS THE POWER OF ALPHA.
0088         DO 133 K=3,21,2
0089  C    THIS IS THE CONFIGURATION OF THE NRHO MODEL (I=1)
0090         D(1,1,K)=2.0*X(1,1,K)
0091         D(1,2,K)=D(1,1,K)+4.0*X(1,2,K)
0092         D(1,3,K)=D(1,2,K)+2.0*X(1,2,K)+10.0*X(1,3,K)+2.0*X(2,1,K)
0093         D(1,4,K)=D(1,3,K)+14.0*X(1,4,K)+6.0*X(2,2,K)+12.0*X(1,5,K)
0094         D(1,5,K)=D(1,4,K)-3.0*X(1,5,K)
0095         D(1,6,K)=D(1,4,K)+6.0*X(1,5,K)+10.0*X(2,3,K)+2.0*X(3,1,K)
0096        1+12.0*X(1,6,K)
0097  C    THIS IS THE CONFIGURATION OF THE EHO MODEL (I=2)
0098         D(2,1,K)=.27094*(X(1,2,K)+6.3819*X(1,1,K))
0099         D(2,2,K)=2.0*(X(1,1,K)+X(1,2,K))+.32814*(X(2,2,K)+5.0949*X(2,1,K))
0100         D(2,3,K)=2.0*(X(1,1,K)+X(1,2,K)+X(2,1,K)+X(2,2,K)+2.0*X(1,2,K)+
0101        1 2.0*X(1,3,K)+X(3,1,K)+X(3,2,K))
0102         D(2,4,K)=D(2,3,K)+4.0*(X(2,2,K)+X(2,3,K))+6.0*(X(1,3,K)+X(1,4,K))
0103        1 +2.0*(X(4,1,K)+X(4,2,K))+4.0*(X(3,2,K)+X(3,3,K))
0104         D(2,5,K)=D(2,4,K)-.47652*(X(3,4,K)+5.29564*X(3,3,K))
0105      133 D(2,6,K)=D(2,4,K)+6.0*(X(2,3,K)+X(2,4,K))+8.0*(X(1,4,K)+X(1,5,K))
0106        1 +.26678*(X(5,2,K)+6.4967*X(5,1,K))
0107         DO 79 I=1,2
0108  C      I=1:NON-RELATIVISTIC; I=2: RELATIVISTIC
0109         IF (I.EQ.2) GO TO 13
0110         WRITE (6,50)
```

```
     00000000011111111112222222222333333333344444444455555555566666666677777777778
     12345678901234567890123456789012345678901234567890123456789012345678901234567890
CARD
0111          GO TO 14
0112       13 WRITE (6,70)
0113       14 DO 79 JK=1,6
0114          KZ=ITER(JK)
0115          WRITE(6,60) KZ
0116          Z=KZ
0117          DO 15 K=3,21,2
0118          KR=K-3
0119          D(I,JK,K)=D(I,JK,K)/Z
0120       15 WRITE (6,30) D(I,JK,K),K,KR
0121     C    THIS EVALUATES THE INTEGRAL: 4PI*INT(RHO*R*R)DR, SUMMED FROM ZERO TO INF.
0122       75 FORMAT (1HO,50X,'NORMALIZATION INTEGRAL = ',F14.6)
0123          CHECK=5.568328*(D(I,JK,3)+1.5*D(I,JK,5)+3.75*D(I,JK,7)+13.125*
0124         1D(I,JK,9)+59.0625*D(I,JK,11)+324.84375*D(I,JK,13)+2111.484375*
0125         2 D(I,JK,15)+15836.133*D(I,JK,17)+134607.1288*D(I,JK,19)+
0126         3 1278767.7255*D(I,JK,21))
0127       79 WRITE (6,75) CHECK
0128     C
0129     C       THIS PROGRAM EVALUATES THE COEFFICIENTS F(I,KZ,M) IN THE FORM FACTOR F(Q)
0130       80 FORMAT (1H1,'********** FORM FACTORS F(Q) **********')
0131       90 FORMAT (1HO,30X,'HARMONIC OSCILLATOR FORM FACTOR')
0132      100 FORMAT (1H1,30X,'RELATIVISTIC FORM FACTORS')
0133      110 FORMAT (1HO,10X,'Z=',I2,5X,'F(Q)= EXP(-Q*Q/(4*A*A)) *')
0134      120 FORMAT (1HO,25X,E17.10,' (Q/A)**',I2)
0135          WRITE (6,80)
0136          DO 25 I=1,2
0137          IF (I.EQ.2) GO TO 16
0138          WRITE (6,90)
0139          GO TO 17
0140       16 WRITE (6,100)
0141       17 DO 25 JK=1,6
0142          KZ=ITER(JK)
0143          WRITE(6,110) KZ
0144          DO 25 M=1,10
0145          MQ=2*M-2
0146     C    G4=GAMMA(2M)
0147          KW=MQ+1
0148          G4=1.0
0149          DO 18 IW=1,KW
0150          G=IW
0151       18 G4=G4*G
0152          SUM=0.0
0153          DO 24 N=M,10
0154     C    G5=GAMMA(2N)
0155          KW=2*N-1
0156          G5=1.0
0157          DO 19 IW=1,KW
0158          G=IW
0159       19 G5=G5*G
0160     C    G6=GAMMA(N-M+1)
0161          KW=N-M
0162          G6=1.0
0163          IF(KW) 23,23,21
0164       21 DO 22 IW=1,KW
0165          G=IW
```

```
      0000000001111111111222222222233333333334444444445555555556666666666777777777 8
      1234567890123456789012345678901234567890123456789012345678901234567890123456789 0
CARD
0166      22 G6=G6*G
0167      23 KM=2*N+1
0168         TERM=(2.0)**(-2*N+2)*G5*D(I,JK,KM)/G6
0169      24 SUM=SUM+TERM
0170         F(I,JK,M)=((-1.0)**(M-1))*5.568328*SUM/G4
0171      25 WRITE (6,120) F(I,JK,M),MQ
0172         STOP
0173         END
0174  $ENTRY
0175        2   6  20  52  49  82
0176  $IBSYS
```

APPENDIX D

One of the many theorems concerning the roots of a polynomial is the Sturm theorem, which gives an easy method of finding the number of roots of a polynomial in any given interval. This theorem is discussed in most any book on higher algebra, and the following discussion is adapted from Mishina (46).

Suppose we are looking for the number of roots of the equation

$$f(x) = a_0 x^0 + a_1 x^1 + a_2 x^2 + a_3 x^3 + \ldots$$

in an interval $a \leq x \leq b$. The procedure is to construct a "Sturm series" and then apply the Sturm theorem at the two end points.

Construction of a Sturm series is done as follows: We take the polynomial $f(x) = f_0(x)$, its derivative $f'(x) = f_1(x)$, then the remainder $r_1(x)$ obtained when $f_0(x)$ is divided by $f_1(x)$, with the opposite sign $[-r_1(x) = f_2(x)]$; then the remainder $r_2(x)$, obtained when $f_1(x)$ is divided by $f_2(x)$, with the opposite sign $[-r_2(x) = f_3(x)]$; then the remainder after the division of $f_2(x)$ by $f_3(x)$, with the opposite sign $[-r_3(x) = f_4(x)]$ ... Having done this, we have constructed a series of polynomials $f_0(x)$, $f_1(x)$, $f_2(x)$, ..., each of degree one less than the preceding.

We can now apply Sturm's theorem and find the number of roots:

The number of distinct real roots of $f(x)$ lying in the interval $[a,b]$ is equal to difference between the number of changes of sign in

the series of $f_o(a)$, $f_1(a)$, $f_2(a)$, ... and the number of changes of sign in the series $f_o(b)$, $f_1(b)$, $f_2(b)$, ...

If we are looking for the number of positive roots of a function $f(x)$, this is very simple to apply, since the sign of $f_n(0)$ is determined solely by the zeroth degree term and the sign of $f_n(\infty)$ is determined solely by the highest degree term, so the number of changes of sign can be determined by inspection, once the Sturm series has been constructed. To construct these series is not a simple matter. The calculations are direct, but very laborious, particularly for a tenth-degree polynomial, as in the case of EHO lead. Fortunately, however, division of one polynomial by another is amenable to computer work, and such a program has already been written and published (60). The work done by the author was to adapt the program PDIV to the Sturm series approach, where the remainder becomes the divisor for the next division. A crude, though workable, program that accomplishes this is presented in this appendix.

The input necessary for each polynomial to be studied consists of two separate entries: the first entry must contain the degree of the polynomial (IDIMX), and the second entry contains the coefficients of the polynomial, ordered from lowest degree to highest degree (a_o, a_1, a_2, ...).

The printed output will list the coefficients in the Sturm polynomials, beginning with $f_o(x)$ [the original polynomial] and proceeding to $f_n(x)$ [a polynomial of degree zero]. Each set of coefficients will be ordered from lowest degree to highest degree. In its present state, the program will print out $f_o(x)$ once, $f_n(x)$ once, but all intervening

polynomials will be repeated:

$[f_o(x)]$

$[f_1(x)]$

$[f_1(x)]$

$[f_2(x)]$

$[f_2(x)]$

$\vdots$

$[f_{n-1}(x)]$

$[f_{n-1}(x)]$

$[f_n(x)]$

For construction of ten series, execution time is less than 6 seconds on the IBM 360/50.

```
      00000000011111111112222222222333333333344444444455555555556666666667777777778
      12345678901234567890123456789012345678901234567890123456789012345678901234567890
CARD
0001  $JOB
0002  C    THIS PROGRAM CONSTRUCTS A STURM SERIES FOR THE POLYNOMIAL F(Z), WHERE
0003  C    F(Z) = X(1,1)*Z**0 + X(1,2)*Z**1 + X(1,3)*Z**2 + ... + X(1,IDIMX)*Z**IDIMX-1
0004        DIMENSION X(20,20),Y(20,20),P(20,20)
0005     20 FORMAT (1HO,10X,'KZ=',I2)
0006        DO 9 KZ=1,10
0007        READ, IDIMX
0008        READ, (X(1,I),I=1,IDIMX)
0009        WRITE (6,20) KZ
0010        DO 1 I=1,IDIMX
0011      1 PRINT, X(1,I)
0012        IDIMY=IDIMX-1
0013        IF (IDIMY.LE.0) GO TO 9
0014        DO 2 I=1,IDIMY
0015        Y(1,I)=I*X(1,I+1)
0016      2 PRINT, Y(1,I)
0017        KL=IDIMY
0018        DO 8 L=1,KL
0019        IDIMP=IDIMX-IDIMY+1
0020        IDIMX=IDIMY-1
0021        IF (IDIMX) 9,9,10
0022     10 I=IDIMP
0023      3 II=I+IDIMX
0024        P(L,I)=X(L,II)/Y(L,IDIMY)
0025        DO 4 K=1,IDIMX
0026        J=K-1+I
0027        X(L,J)=X(L,J)-P(L,I)*Y(L,K)
0028      4 CONTINUE
0029        I=I-1
0030        IF (I) 5,5,3
0031      5 CONTINUE
0032        IDIMX=IDIMY
0033        DO 6 M=1,IDIMX
0034        X(L+1,M)=Y(L,M)
0035      6 PRINT, X(L+1,M)
0036        IDIMY=IDIMX-1
0037        DO 7 M=1,IDIMY
0038        Y(L+1,M)=-X(L,M)
0039      7 PRINT, Y(L+1,M)
0040      8 CONTINUE
0041      9 CONTINUE
0042        STOP
0043        END
0044  $ENTRY
0045  1
0046  0.1E01
0047  2
0048  0.1000025E 01   -0.144092E00
0049  2
0050   0.1E 01        -0.1111111E 00
0051  4
0052  0.9999969E 00   -.2131056E 00   .2782075E-01    -0.1161E-02
0053  3
0054   0.1E 01        -0.25E 00       0.1249999E-01
0055  6
```

```
      0000000001111111112222222222333333333344444444455555555566666666677777777778
      1234567890123456789012345678901234567890123456789012345678901234567890123456789
CARD
0056  0.1000002E 01   -.3499999E 00   .6333333E-01   -.5773801E-02   .2529753E-03
0057  -.3720233E-05
0058  5
0059   0.9999996E 00  -0.4285713E 00  0.489758E-01   -0.1724974E-02  0.1214771E-04
0060  8
0061  .10E 01         -.5084226E 00   .1196635E 00   -.1419339E-01   .8897951E-03
0062  -.2795927E-04   .4019545E-06   -.2191776E-08
0063  6
0064   0.9999996E 00  -0.5487802E 00  0.8841449E-01  -0.5299065E-02  0.1119095E-03
0065  -0.4399394E-06
0066  10
0067  .10E 01         -.6051865E 00   .1570771E 00   -.2237544E-01   .2008361E-02
0068  -.1209193E-03   .4876324E-05   -.1238519E-06   .1751794E-08    -.1034201E-10
0069  $IBSYS
```

APPENDIX E

Evaluation of F(q), $\frac{d\sigma}{d\Omega}$ as a function of θ . This program is a simple evaluation of two functions, each having the scattering angle θ as its dependent variable. In this program, θ is runs from 2^{o} to 178^{o}, incrementing by steps of 2^{o}. At each value of θ, the momentum transfer q, the form factor F(q), and the cross-section ($d\sigma/d\Omega$) are evaluated and printed. The input required for this program consists of two entries: the vector of coefficients C(K,M) in the form factor, ordered from zeroth degree to tenth degree; and numerical values for the four constants B(K,1), B(K,2), B(K,3), and α(K) [all expressed in CGS units.] The constants are defined as follows:

$$B(K,1) = \frac{2E_o}{Mc^2}$$

$$B(K,2) = \left(\frac{Ze^2}{2E_o}\right)^2$$

$$B(K,3) = \frac{2E_o}{c\hbar}$$

$$\alpha(K) = \sqrt{\frac{m_o \omega_K}{\hbar}}$$

When CGS units are used for these parameters, $d\sigma/d\Omega$ will have units of [cm^2/steradian].

The execution time is approximately 5 seconds per nucleus.

```
     00000000011111111112222222222333333333344444444455555555556666666666777777777 8
     12345678901234567890123456789012345678901234567890123456789012345678901234567890
CARD
0001 $JOB
0002 C      THIS PROGRAM EVALUATES THE FORM FACTOR AND DIFFERENTIAL CROSS-
0003 C      SECTION FOR ELASTIC SCATTERING
0004        DIMENSION C(20,20),B(20,5),ALPHA(20)
0005     10 FORMAT (5E16.7/5E16.7/F15.7,E16.5,E16.7,E10.4)
0006     20 FORMAT (1H1,50X,'K=',I2)
0007     30 FORMAT (1HO,    'LAB ANGLE (DEGREES)',43X,'FORM FACTOR',10X,
0008       1'ELECTRON SCATTERING CROSS-SECTION')
0009     40 FORMAT ( 5X,'THETA=',I3,17X,'Q=',E14.7,17X,'FQ=',E14.7,17X,
0010       1'DSIGMA=',E14.7,5X,I3)
0011        READ (5,10) ((C(K,M),M=1,10),(B(K,I),I=1,3),ALPHA(K),K=1,02)
0012        DO 2 K=1,2
0013        WRITE (6,20) K
0014        WRITE (6,30)
0015        DO 2 I=2,178,2
0016        THETA=I
0017        PHI=THETA/114.591559
0018        COSPHI=COS(PHI)
0019        SINPHI=SIN(PHI)
0020        ZETA=SQRT(1.0+B(K,1)*SINPHI*SINPHI)
0021        Q=B(K,3)*SINPHI/ZETA
0022        Y=Q*Q/(ALPHA(K)*ALPHA(K))
0023        SUM=0.0
0024        DO 1 M=1,10
0025        TERM=C(K,M)*Y**(M-1)
0026      1 SUM=SUM+TERM
0027        FQ=SUM*EXP(-Y/4.0)
0028        DSIGMA=B(K,2)*COSPHI*COSPHI*FQ*FQ/(SINPHI*SINPHI*SINPHI*SINPHI*
0029       1 ZETA*ZETA)
0030      2 WRITE (6,40) I,Q,FQ,DSIGMA,I
0031        STOP
0032        END
0033 $ENTRY
0034  0.9999996E 00  -0.5487802E 00   0.8841449E-01   -0.5299065E-02   0.1119095E-03
0035 -0.4399394E-06  0.0             0.0              0.0              0.0
0036 0.00256033      5.666667E-28    2.51366E 13      3.71E12
0037 .10E 01          -.6051865E 00   .1570771E 00     -.2237544E-01    .2008361E-02
0038 -.1209193E-03    .4876324E-05    -.1238519E-06    .1751794E-08     -.1034201E-10
0039 0.00256033      5.666667E-28    2.51366E 13      3.71E12
0040 $IBSYS
```

VITA

2

Jeffrey John Braun

Candidate for the Degree of

Master of Science

Thesis: A STUDY OF THE NUCLEUS USING RELATIVISTIC WAVE FUNCTIONS

Major Field: Physics

Biographical:

Personal Data: Born in Elgin, Illinois, August 7, 1945, the son of Arnold Fred and Garnet Kanies Braun.

Education: Attended Knox College, Galesburg, Illinois, and received the Bachelor of Arts degree with a major in physics in June 1967; completed the requirements for the Master of Science degree in May, 1970.

Professional Experience: Employed as a graduate assistant in physics at OSU from 1967 to 1970.